Electronic Supplementary Material (ESI) for Dalton Transactions.
This journal is © The Royal Society of Chemistry 2024

Electronic Supplementary Information

The first example of polymeric lanthanide *tetrakis*-trifluoroacetates in chemical solution deposition of up-converting $NaGdF_4$: Yb, Er, Nd thin film

Maria Burlakova,[a] Daria Blinnikova [b], Gleb Volkonovskiy [a], Haoyang Chai [b, c], Dimitry Grebenyuk [a, c] and Dmitry Tsymbarenko [*a]

a. Department of Chemistry, Lomonosov Moscow State University, Moscow 119991, Russia.

b. Faculty of Materials Science, Lomonosov Moscow State University, Moscow 119991, Russia.

c. Faculty of Materials Science, MSU-BIT University, Shenzhen 518172, China.

**E-mail: tsymbarenko@gmail.com; tsymbarenko@inorg.chem.msu.ru*

Content

1. Synthesis of $(detaH_2)_n[Ln_2(tfa)_8]_n$.

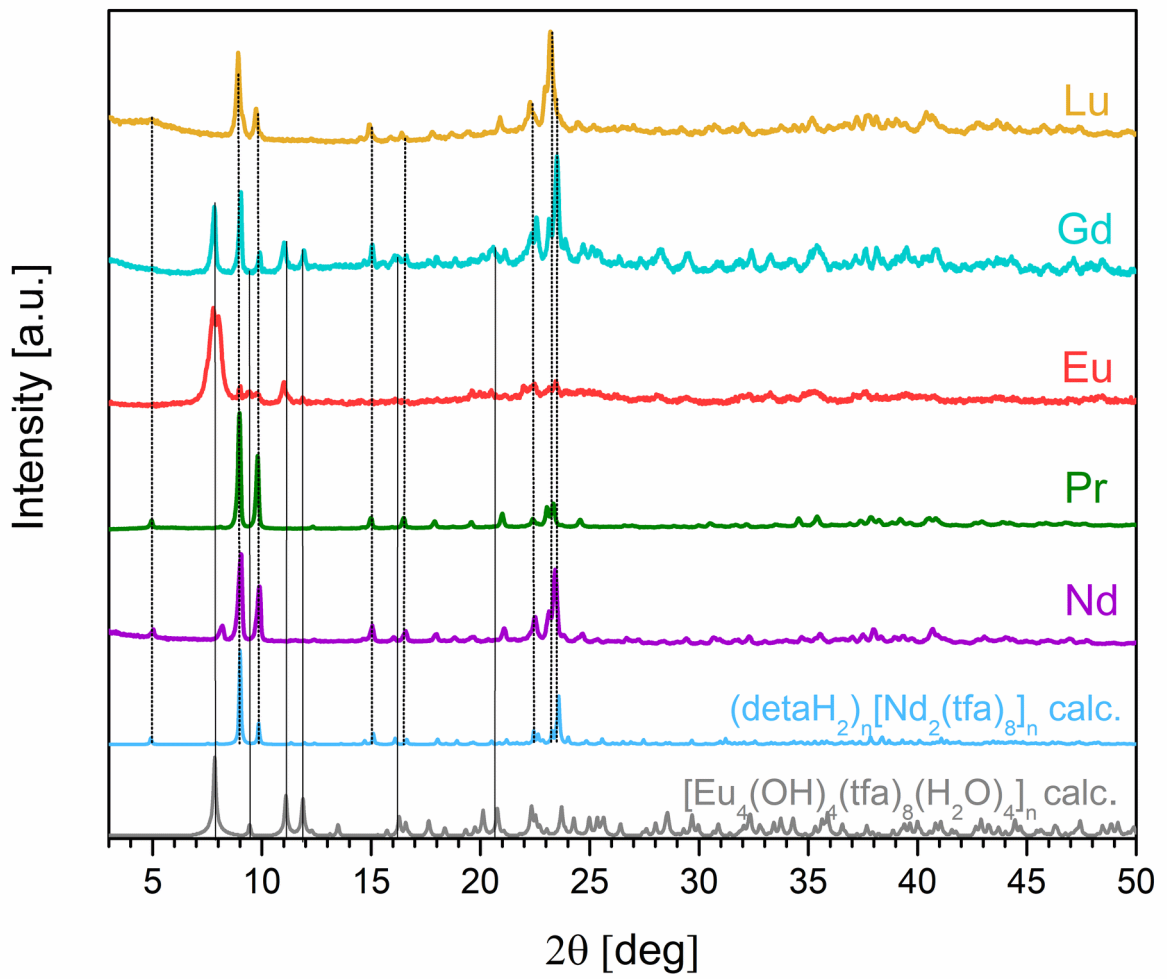

Figure S1. PXRD data for powder samples which contain complexes $(detaH_2)_n[Pr_2(tfa)_8]_n$ (**2**), $(detaH_2)_n[Eu_2(tfa)_8]_n$ (**5**), $(detaH_2)_n[Gd_2(tfa)_8]_n$ and $(detaH_2)_n[Lu_2(tfa)_8]_n$ and calculated data for $(detaH_2)_n[Nd_2(tfa)_8]_n$ and $[Eu_4(OH)_4(tfa)_8(H_2O)_4]\cdot 2H_2O$. The dashed black lines show some peaks of $(detaH_2)_n[Nd_2(tfa)_8]_n$ with high intensity. Black solid and dotted lines trace some intense peaks of $[Eu_4(OH)_4(tfa)_8(H_2O)_4]\cdot 2H_2O$ and $(detaH_2)_n[Nd_2(tfa)_8]_n$ respectively.

2. X-ray crystallography

Table S1. Crystallographic data for **1**-**3** and **6**-**9**

Compound	**1**	**2**	**3**	**6**	**7**	**8**	**9**
Formula	$La_4C_{50}H_{49}F_{48}N_{11}O_{34}$	$Pr_2C_{20}H_{15}F_{24}N_3O_{16}$	$Nd_2C_{20}H_{15}F_{24}N_3O_{16}$	$LaC_8H_5F_9NO_7$	$GdC_{17}H_{34}F_9N_6O_7$	$YbC_{14}H_{26}F_9N_6O_6$	$C_8H_{15}F_6N_3O_4$
Formula weight	2815.64	1291.17	1297.83	537.04	762.75	718.45	331.23
Diffractometer	Bruker D8 Quest	Bruker D8 Quest	Bruker D8 Quest	Bruker D8 Quest	Bruker D8 Quest	Bruker D8 Quest	Bruker APEX II
Data collection method	*ω*-scans	*ω*-scans	*ω*-scans	*ω*-scans	*ω*-scans	*ω*-scans	*ω*-scans
Temperature (K)	100(2)	100(2)	100(2)	100(2)	100(2)	100(2)	120(2)
Crystal system	Monoclinic	Orthorhombic	Orthorhombic	Monoclinic	Monoclinic	Monoclinic	Triclinic
Space group	*P2₁*	*Pbca*	*Pbca*	*P2₁/c*	*C2/c*	*P2₁/c*	P$\bar{1}$
a (Å)	8.783(3)	8.633(3)	8.6514(16)	12.4741(13)	18.294(7)	9.5390(7)	9.799(2)
b (Å)	23.995(8)	23.337(16)	23.450(5)	12.8468(12)	12.580(5)	28.4276(19)	10.499(2)
c (Å)	21.910(7)	35.961(19)	35.880(6)	9.7054(9)	24.686(10)	8.5495(6)	14.933(3)
α (°)	90	90	90	90	90	90	69.922(4)
β (°)	91.324(12)	90	90	100.300(4)	101.007(7)	90.018(2)	76.226(5)
γ (°)	90	90	90	90	90	90	72.531(4)
V (Å^3)	4616(3)	7245(7)	7279(2)	1530.2(3)	5577(4)	2318.4(3)	1360.6(5)
Z	2	8	8	4	8	4	4
Colour, habit	Colourless, needle	Green, needle	Pale violet, needle	Colourless, plate	Colourless, plate	Colourless, block	Colourless, plate
Crystal dimensions (mm)	0.190×0.030×0.020	0.162×0.047×0.035	0.260×0.019×0.016	0.239×0.072×0.039	0.293×0.191×0.022	0.116×0.083×0.059	0.179×0.133×0.052
Dcalc (g·cm^{-3})	2.026	2.367	2.368	2.331	1.817	2.058	1.617
μ (mm^{-1})	1.993	2.855	3.017	2.929	2.485	4.150	0.176
Unique reflections (R_{int})	16111 (0.1671)	8052 (0.3385)	7870 (0.1208)	3685(0.0529)	6531(0.0934)	5041(0.0566)	6426 (0.0374)
Observed reflections [I > 2σ(I)]	8668	2761	5110	3165	5991	4746	3504
Parameters, restrains	1330, 233	589, 30	588, 31	236, 0	419, 166	326, 54	389, 0
R_1[I > 2σ(I)], ωR^2	0.0760, 0.1451	0.0806, 0.1709	0.0507, 0.1220	0.0281, 0.0636	0.1027, 0.2873	0.0570, 0.1163	0.0599, 0.1297
Goodness-of-fit on F^2	0.994	0.919	0.932	1.007	1.131	1.272	1.011
Absorption correction	SADABS	SADABS	SADABS	SADABS	SADABS	SADABS	SADABS
T_{min}, T_{max}	0.6035, 0.8620	0.5037, 1.0000	0.5406, 0.8763	0.6223, 0.7473	0.3978, 1.0000	0.6443, 0.7459	0.7546, 1.0000
ρ_{min}, ρ_{max} (eÅ^{-3})	-1.358, 2.060	-1.334, 1.309	-0.872, 1.220	-0.830, 1.065	-4.148, 3.111	-3.797, 4.014	-0.605, 0.848

2.1. Comments on data collection and structure refinement

*2.1.1. Structure of {(detaH$_2$)$_2$[La$_2$(tfa)$_8$]$_2$·5CH$_3$CN·2H$_2$O}$_n$ (**1**).*

The single crystal of **1** was a tiny needle of 0.020 mm in diameter with weak scattering power and it also susceptible to radiation damage. The diffraction data were collected at an exposition time of 90 sec per frame. The structure is based on weak data (I/σ(I) = 4.4), but the resulted residual density and chemical connectivity are reasonable (**Figure S2a**). The R_{int} value 16.7% is higher than recommended <12% (**Figures S2b-S2d**). The reasons for larger R_{int} are sample radiation damage and weak scattering power which is complicated by racemic twinning.

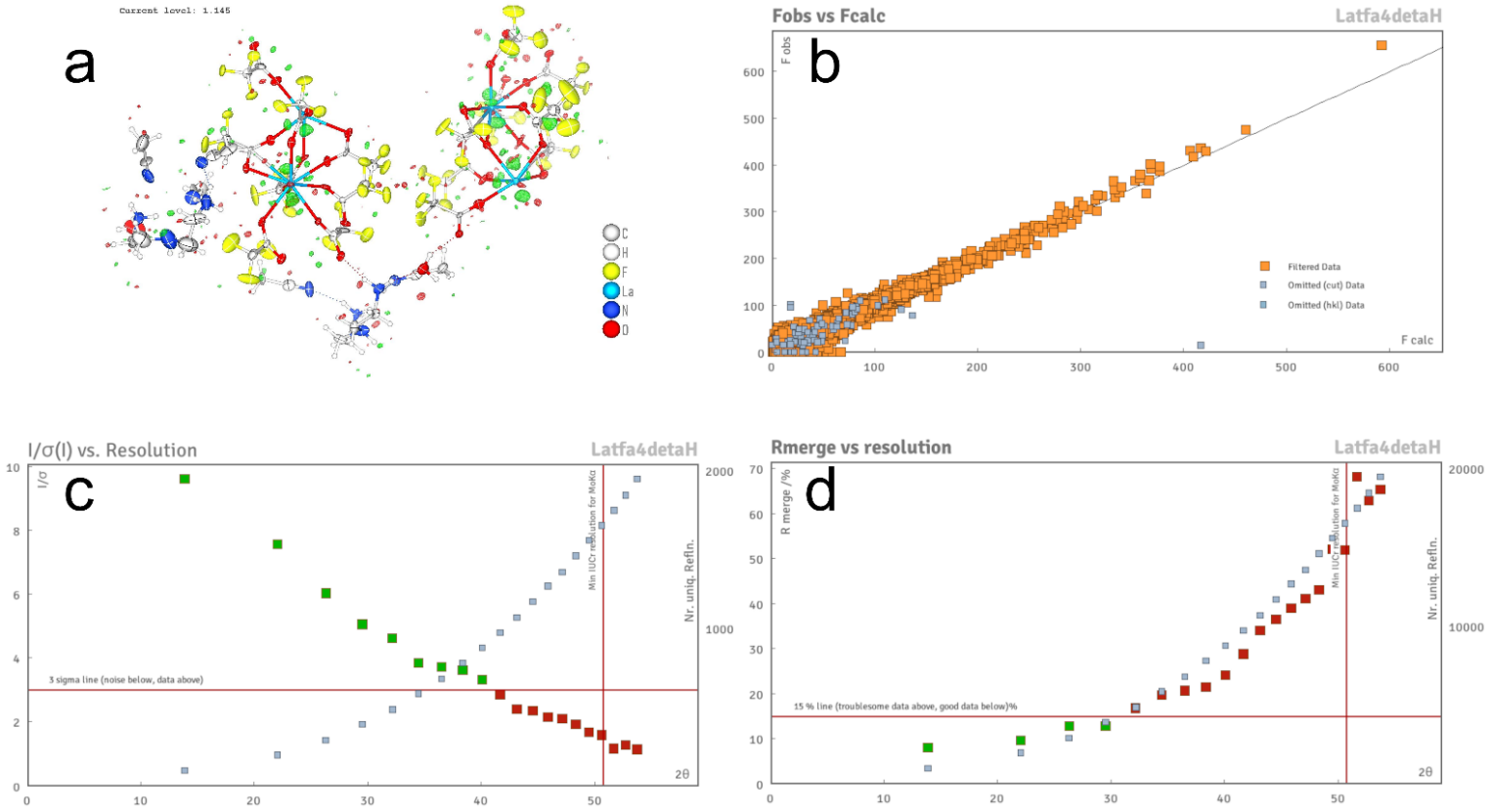

Figure S2. Indicators of data quality of structure **1**: residual electron density map (a), F_{obs} and F_{calc} correlation (b), Intensity over dispersion statistic (c), merging R-factor (d).

*2.1.2. Structure of $(detaH_2)_n[Pr_2(tfa)_8]_n$ (**2**).*

The compound (**2**) crystallizes in a form of tiny needle-like crystals of 0.040 mm in diameter with weak scattering power. The diffraction data were collected using Sensitive mode of PHOTON III detector at an acquisition time of 60 seconds per frame. This long acquisition time, high sensitivity of Photon III detector and high brightness of ImuS 3.0 source allowed us to observe the remarkable peaks at least up to the resolution of 0.78 Å (**Figure S3**). Unfortunately, these tiny crystals were strongly affected by the radiation damage during exposition even at 100K and loose their scattering power after 150 frames (**Figure S3**). This effect makes unwise to further increase the exposition time since this resulted in fewer meaningful frames. To achieve the required data completeness we have set up the second crystal collect another peace of the required diffraction dataset. Two datasets were integrated independently within a meaningful omega range. Data were corrected for absorption using crystal shape, for crystal decay and than combined together to deliver final HKL file using SADABS. This 'trick' allowed us to reach the required data completeness (99.6%) but R_{int} is rather high (33.8%). Nevertheless, we have obtained acceptable values of R_1 (<9%), bond precision (sigma(C-C) ~ 0.03 Å) and perfect residual density +1.309/-1.334 e/A^{-3} (**Figure S4**). We were able improve the Rint value down to 28% by excluding some partially decayed frames without loss of the data completeness (97%), but this resulted in significantly worse bond precision (sigma(C-C) ~ 0.041 Å). Therefore, finally we decided to sacrifice R_{int} to get better analysis accuracy. Such crystallographic approach for tiny needle-like crystals of related compounds affected by radiation damage was previously applied by us for synchrotron diffraction datasets [1]. Additionally, the correctness of the refined structure was confirmed by the isostructural Nd analog **4** that showed better diffraction.

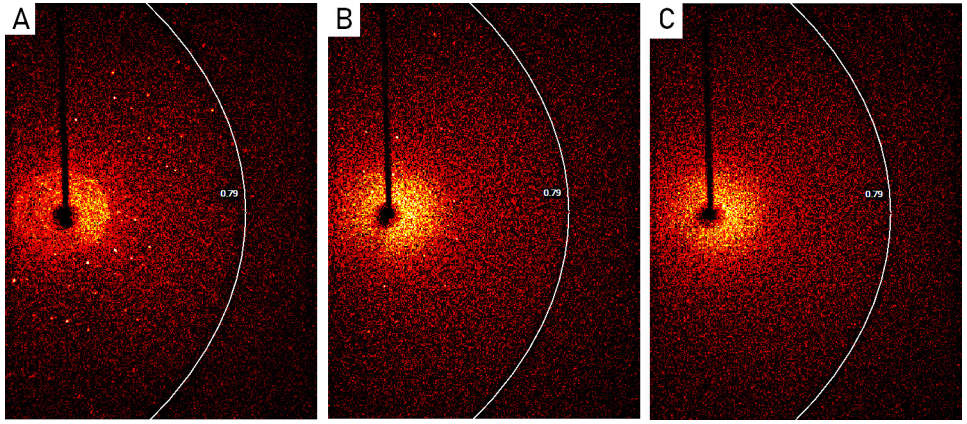

Figure S3. Diffraction patterns of $(detaH_2)_n[Pr_2(tfa)_8]_n$ (**2**) single crystal collected at 100 K with the exposition time of 60 sec/frame within one omega-scan. Data are affected by radiation damage: (A) early frame shows detectable peaks up to 0.78 Å resolution; (B) frame after 150 minutes acquisition shows only few bright peaks; (C) no peaks are detectable after 200 minutes of acquisition.

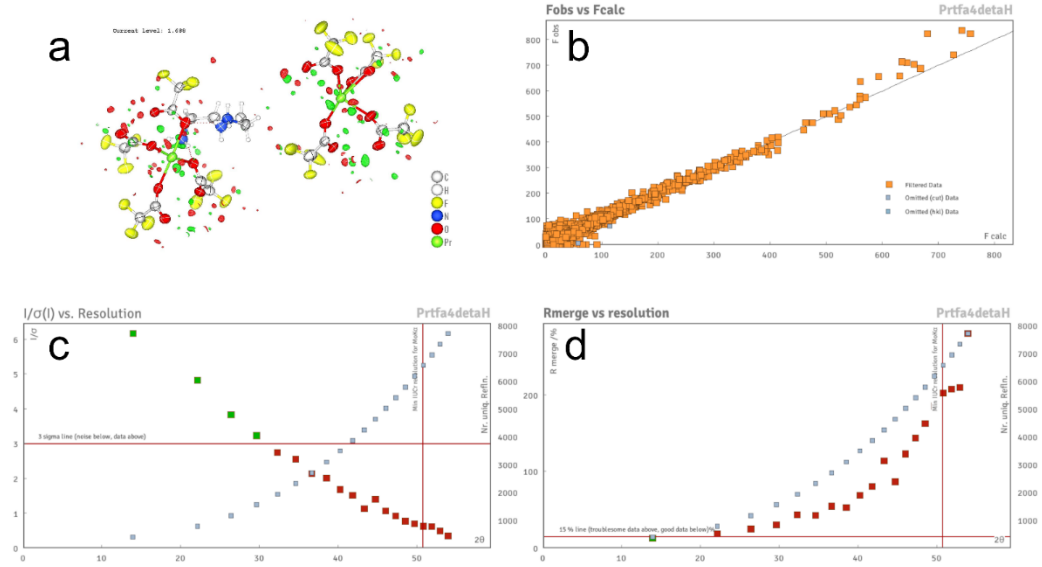

Figure S4. Indicators of data quality of structure **2**: residual electron density map (a), F_{obs} and F_{calc} correlation (b), Intensity over dispersion statistic (c), merging R-factor (d).

*2.1.3. Structure of $(detaH_2)_n[Nd_2(tfa)_8]_n$ (**3**).*

The spurious bonds have been removed. Concerning the resolution and I/sigma(I). The crystals of this compound have a similar needle-like shape as **3** and were also susceptible to radiation damage, although not as much as the Pr analogue. The diffraction data were also collected using the long exposition as high as 60 sec per frame. Indeed, the data between 0.74 and 0.84 Å are rather weak, but inclusion of these peaks into refinement allowed us to achieve better accuracy (e.g. sigma(C-C) ~ 0.010 Å) and only slightly increased R-factors (R_1 = 5.3%) with the respect to data limited by 0.84 Å resolution (sigma(C-C) ~ 0.012 Å, R_1 = 4.7%) or by 0.78 Å resolution (sigma(C-C) ~ 0.011 Å, R_1 = 5.1%) (**Figure S5**). In the revised manuscript we have re-refined the structure with 0.78 Å resolution limit to address the reviewer comment.

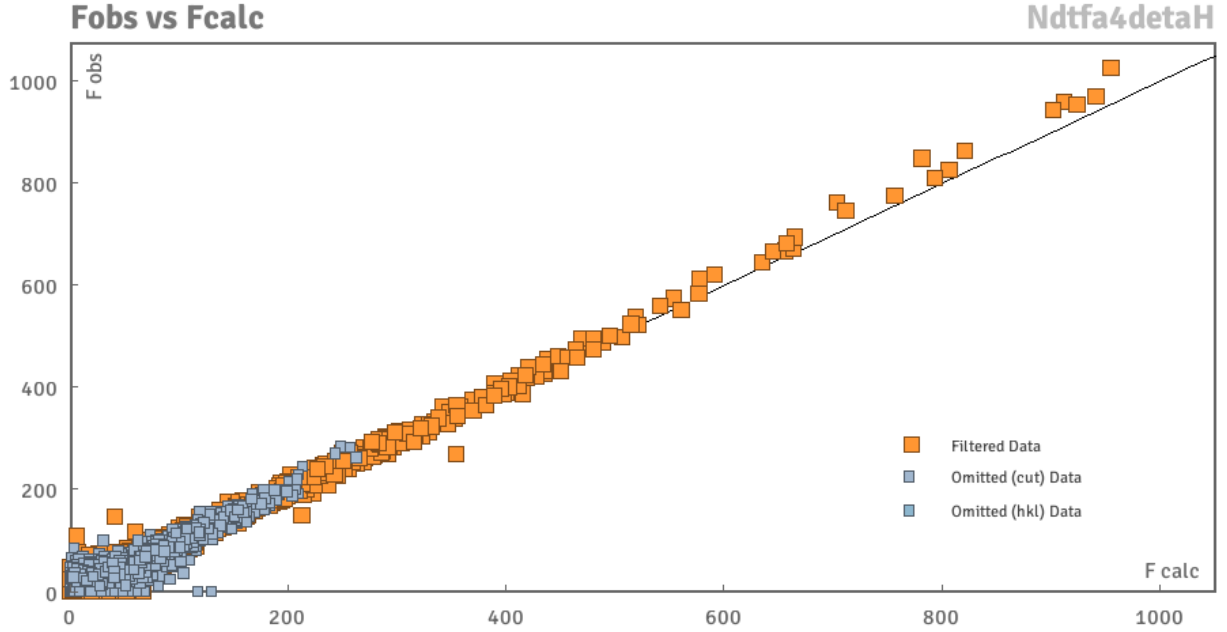

Figure S5. F_{obs} and F_{calc} correlation for structure **3**.

*2.1.4. Structure of [Gd(tfa)$_3$(deta)$_2$](iPrOH) (**7**).*

The compound (**7**) crystallizes in a form of very thin plate-like crystals with high anisotropy and tends to form splices and twins. We have done all our best to growth and harvest the best crystal, to collect the best diffraction data and to refine the structure with the highest available precision. We have harvested and selected crystals using polarization microscope and verified their quality using the diffractometer. The best available crystal was a plate with the lateral size of 0.191x0.293 mm and the thickness of only 0.022 mm. Crystal shows noticeable diffraction pattern at least up to resolution of 0.78 Å (**Figure S6**).

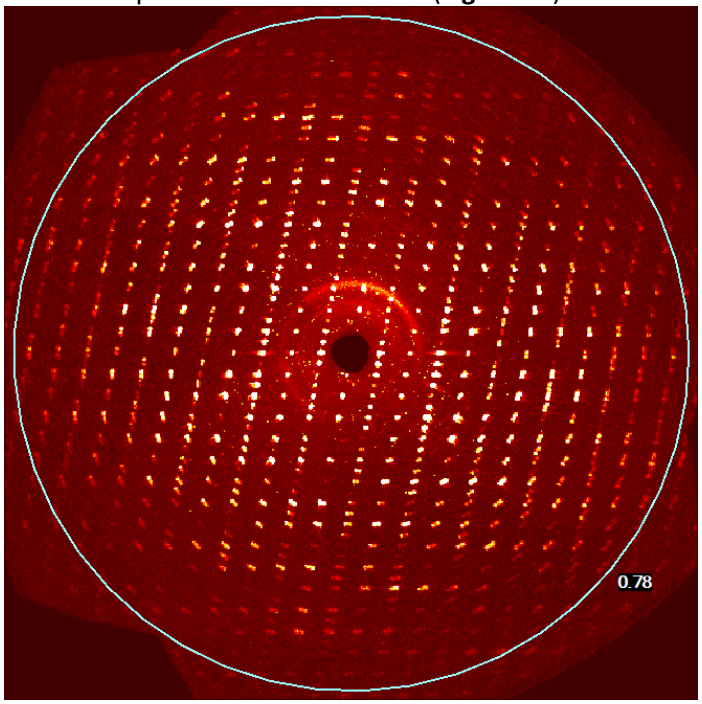

Figure S6. Reconstructed diffraction plane *(h0l)* of [Gd(tfa)$_3$(deta)$_2$](^{i}PrOH) (**7**).

Indexation the diffraction pattern revealed that the crystal consists of at least 4 components and combines pseudo-merohedral twinning and "random" twinning with slight (by 1.8 deg) mutual rotation. These "random" blocks could not be separated from each other physically without crushing the crystal. Therefore, we have collected the full experiment with the detailed omega-scans (omega step 0.4°) and tried various techniques for processing of twinned data:

(i) indexing of the components with cell now followed by integration of multi-crystals has not resulted in good data due to strong overlapping and unstable orientation matrices refinement, (ii) integration with the big spot size also has failed in large residual density at the structure refinement stage, (iii) finally we have performed integration with reduced spot size to overcome the spots overlapping and have obtained the best dataset. We have performed the optimization of spot size and size of 0.6×0.6×1.2º gives the best results allowing to reduce the non-merohedral twinning effect, but unfortunately this 'trick' artificially reduces the I/σ(I). After the structure solution we have analyzed the data by TwinRotMat algorithm to reveal the merohedral twinning and to de-twin the dataset with the PLATON. Finally, the refinement against the de-twinned data has revealed the disordered isopropanol molecules within the cavities. We have excluded these solvent molecules by SQUEEZE procedure of PLATON [2]. The analysis of resulted residual electron density revealed the highest negative peak of -4.15 eÅ^{-3} at (0.2275, 0.9222, 0.1501) is located above the heavy Gd1$^{(1-x,\ y,\ 0.5-z)}$ atom (0.2301, 0.3604, 0.1514) in *ac* plane. Negative peak is located at 1.705Å from the nearest O6 atom, so this peak can not be attributed to any chemically sensible structural reason. The most

likely reason for higher than expected value of negative residual density is the under-accounted twinning effect. Two highest positive residual density peaks are of 3.11 and 2.78 eÅ^{-3} and are located in the vicinity of heavy Gd1 atom (at 0.936 and 0.909 Å respectively) that is typically attributed to Fourier ripples and not ideal absorption correction, which is problematic for twinned data. It worth noting that both positive and negative residual density peaks do not exceed 0.1*Zmax criterion (6.4 eÅ-3, Zmax = 64 for Gd) and do not generate A-, B- and even C-level alerts of PLATON/CheckCIF test.

*2.1.5. Structure of [Yb(tfa)$_2$(deta)$_2$](tfa) (**8**).*

The diffraction data for compound (**8**) was integrated as pseudo-merohedral twin. The TwinRotMat algorithm of PLATON[2] was applied to reveal the appropriate twin law. The refinement with 'TWIN -1 0 0 0 -1 0 0.001 0 1' instruction within the SHELXL-2018 software resulted in BASF parameter of 0.45144 and significantly reduced the R-factors (e.g. R1 changed from 23.6 to 5.7%) and residual electron density (reduced from -32.0/+17.0 to -3.8/+4.0 eÅ-3). The negative residual density peak of -3.8 eÅ-3 is located at 1.67Å from N5 atom and at 1.82Å from heavy Yb1 atom, this peak can not be attributed to any chemically sensible structural reason. The most likely reason for higher than expected value of negative residual density is the under-accounted twinning effect. Two highest positive residual density peaks of 4.0 and 3.0 eÅ-3 are located in the vicinity of heavy Yb1 atom (at 0.93 and 0.88 Å respectively) that is typically attributed to Fourier ripples and not ideal absorption correction, which is problematic for twinned data. It worth noting that both positive and negative residual density peaks do not exceed 0.1*Zmax criterion (7 eÅ-3, Zmax = 70 for Yb) and do not generate A-, B- and even C-level alerts of PLATON/CheckCIF test.

Table S2. Continuous Shape Measures (CShM) analysis for La1-La4 in complex **1**.

Structure [ML_8]	OP-8	HPY-8	HBPY-8	CU-8	SAPR-8	TDD-8	JGBF-8	JETBPY-8	JBTPR-8	BTPR-8	JSD-8	TT-8	ETBPY-8
La1	25.963	23.922	17.160	10.366	0.206	2.120	15.951	26.302	2.573	1.915	4.724	11.110	22.315
La2	25.927	23.724	17.365	10.755	0.173	2.376	16.001	26.740	2.519	1.844	4.795	11.600	22.079
La4	26.462	22.974	17.249	10.800	0.177	2.394	16.323	26.423	2.591	1.838	5.054	11.474	22.471
Structure [ML_9]	EP-9	OPY-9	HBPY-9	JTC-9	JCCU-9	CCU-9	JCSAPR-9	CSAPR-9	JTCTPR-9	TCTPR-9	JTDIC-9	HH-8	MFF-9
La3	36.896	22.184	17.883	16.730	10.061	9.819	1.187	1.062	3.253	2.127	13.737	10.535	0.736

Table S3. Continuous Shape Measures (CShM) analysis Ln1 and Ln2 in complex **2**-**3.**

Structure [ML_8]	OP-8	HPY-8	HBPY-8	CU-8	SAPR-8	TDD-8	JGBF-8	JETBPY-8	JBTPR-8	BTPR-8	JSD-8	TT-8	ETBPY-8
Pr1	31.073	21.133	14.422	9.967	1.495	2.790	14.996	25.308	3.836	2.978	5.806	10.612	20.875
Pr2	26.262	23.859	17.592	10.652	0.050	2.509	16.802	27.983	2.710	2.124	5.114	11.494	23.490
Nd1	30.562	20.789	14.907	10.093	1.312	2.722	15.375	25.454	3.483	2.700	5.663	10.765	21.017
Nd2	26.442	24.108	17.813	10.670	0.044	2.485	16.844	28.166	2.782	2.091	5.147	11.482	23.715

[1] Reference shapes abbreviations:
Eight-vertex polyhedra: OP-8 – D_{8h} octagon; **HPY-8** – C_{7v} heptagonal pyramid; HBPY-8 – D_{6h} hexagonal bipyramid; **CU-8** – O_h cube; **SAPR-8** – D_{4d} square antiprism; **TDD-8** – D_{2d} triangular dodecahedron; **JGBF-8** – D_{2d} Johnson gyrobifastigium J26; **JETBPY-8** – D_{3h} Johnson elongated triangular bipyramid J14; **JBTPR-8** – C_{2v} biaugmented trigonal prism J50; **BTPR-8** – C_{2v} biaugmented trigonal prism; **JSD-8** – D_{2d} snub diphenoid J84; **TT-8** – T_d triakis tetrahedron; **ETBPY-8** – D_{3h} elongated trigonal bipyramid.
Nine-vertex polyhedra: **EP-9** – D_{9h} enneagon; **OPY-9** – C_{8v} octagonal pyramid; **HBPY-9** – D_{7h} heptagonal bipyramid; **JTC-9** – C_{3v} Johnson triangular cupola J3; **JCCU-9** – C_{4v} capped cube J8; **CCU-9** – C_{4v} spherical-relaxed capped cube; **JCSAPR-9** – C_{4v} capped square antiprism J10; **CSAPR-9** – C_{4v} spherical capped square antiprism; **JTCTPR-9** – D_{3h} Tricapped trigonal prism J51; **TCTPR-9** – D_{3h} spherical tricapped trigonal prism; **JTDIC-9** – C_{3v} tridiminished icosahedron J63; **HH-9** – C_{2v} Hula-hoop; **MFF-9** – C_s Muffin.

Table S4. Continuous Shape Measures (CShM) analysis for La1 in complex **6**.

Structure [ML_8]	OP-8	HPY-8	HBPY-8	CU-8	SAPR-8	TDD-8	JGBF-8	JETBPY-8	JBTPR-8	BTPR-8	JSD-8	TT-8	ETBPY-8
La1	30.228	24.204	15.643	12.929	2.764	1.461	11.826	27.020	1.591	1.135	2.897	13.320	23.743

Table S5. Continuous Shape Measures (CShM) analysis for Gd1 in complex **7**.

Structure [ML_9]	EP-9	OPY-9	HBPY-9	JTC-9	JCCU-9	CCU-9	JCSAPR-9	CSAPR-9	JTCTPR-9	TCTPR-9	JTDIC-9	HH-8	MFF-9
Gd1	36.420	21.612	19.847	14.983	10.967	9.761	1.663	0.664	1.986	0.725	12.190	12.072	1.132

Table S6. Continuous Shape Measures (CShM) analysis for Yb1 in complex **8**.

Structure [ML_8]	OP-8	HPY-8	HBPY-8	CU-8	SAPR-8	TDD-8	JGBF-8	JETBPY-8	JBTPR-8	BTPR-8	JSD-8	TT-8	ETBPY-8
Yb1	28.635	24.540	16.225	11.938	1.502	0.978	12.702	29.223	1.966	1.749	2.427	12.391	24.801

[1] Reference shapes abbreviations:
Nine-vertex polyhedra: **EP-9** – D_{9h} enneagon; **OPY-9** – C_{8v} octagonal pyramid; **HBPY-9** – D_{7h} heptagonal bipyramid; **JTC-9** – C_{3v} Johnson triangular cupola J3; **JCCU-9** – C_{4v} capped cube J8; **CCU-9** – C_{4v} spherical-relaxed capped cube; **JCSAPR-9** – C_{4v} capped square antiprism J10; **CSAPR-9** – C_{4v} spherical capped square antiprism; **JTCTPR-9** – D_{3h} Tricapped trigonal prism J51; **TCTPR-9** – D_{3h} spherical tricapped trigonal prism; **JTDIC-9** – C_{3v} tridiminished icosahedron J63; **HH-9** – C_{2v} Hula-hoop; **MFF-9** – C_s Muffin.
Eight-vertex polyhedra: OP-8 – D_{8h} octagon; **HPY-8** – C_{7v} heptagonal pyramid; HBPY-8 – D_{6h} hexagonal bipyramid; **CU-8** – O_h cube; **SAPR-8** – D_{4d} square antiprism; **TDD-8** – D_{2d} triangular dodecahedron; **JGBF-8** – D_{2d} Johnson gyrobifastigium J26; **JETBPY-8** – D_{3h} Johnson elongated triangular bipyramid J14; **JBTPR-8** – C_{2v} biaugmented trigonal prism J50; **BTPR-8** – C_{2v} biaugmented trigonal prism; **JSD-8** – D_{2d} snub diphenoid J84; **TT-8** – T_d triakis tetrahedron; **ETBPY-8** – D_{3h} elongated trigonal bipyramid.

*2.2. Crystal structure of {(detaH$_2$)$_2$[La$_2$(tfa)$_8$]$_2$·5CH$_3$CN·2H$_2$O}$_n$ (**1**)*

The asymmetric part of monoclinic unit cell of **1** contains two anionic chains $[La_2(tfa)_8]_n^{2n-}$, two cationic species detaH$_2^{2+}$, and five CH$_3$CN and two H$_2$O solvating molecules. Anionic chains of both types contain pairs of La atoms (La1, La2, and La3, La4), demonstrate roughly similar geometry (Scheme 1) but remarkably differ in La–O interatomic distances. Within the first chain (Figure S4*a*) atoms La1 and La2 with CN being equal to 8 are in square antiprismatic environment (CShM = 0.206 and 0.173 respectively) (**Table S2**). Namely, La1 is coordinated by O1, O3, O5, O7, O9, O11, O13 and O16^{i} atoms (mean La1–O distance 2.532(13) Å) of eight distinct μ^2-κ^1:κ^1-carboxylate groups. Similarly La2 is coordinated by O2, O4, O6, O8, O10^{ii}, O12^{ii}, O14^{ii} and O15 atoms (mean La2–O distance 2.529(18) Å) of the same eight μ^2-κ^1:κ^1-carboxylate groups or their equivalents. Additionally, weak elongated contacts La1···O2 (3.033(17) Å) and La2···O13^{ii} (2.995(17) Å) reveal two carboxylate groups with slightly expressed chelate-bridging coordination (**Table S7**). On the other hand, atoms La3 and La4 within the second chain (Figure S4*b*) possess the different coordination environment. La3 is coordinated by O19, O21, O23, O25, O27, O29, O32^{ii} atoms (mean La3–O distance 2.502(13) Å) of seven μ^2-κ^1:κ^1-carboxylate groups, and O17 and O18 atoms of a μ^2-κ^2:κ^1-carboxylate group. It worth noting that La3–O18 distance (2.882(17) Å) is slightly longer than typical La–O contact that allows one to consider it as weak coordination bond, therefore the CN of La3 equals to 8+1 and the coordination polyhedron of La3 is best described as distorted muffin (CShM = 0.736, **Table S2**). La4 is coordinated by O18, O20, O22, O24, O26^{i}, O28^{i}, O30^{i} and O31 atoms (mean La4–O distance 2.513(19) Å) of eight μ^2-κ^1:κ^1-carboxylate groups (Table S8). Besides, the contacts La4···O29^{i} (3.164(17) Å) and La4···O21 (3.083(17) Å) are remarkably longer and weaker than typical for chelate-bridging coordination, so the CN of La4 equals to 8 and the coordination polyhedron of La4 is best described as square antiprism (CShM = 0.177, **Table S2**, **Figure S7**).

The chains of both types are packed parallel to neighbours along *[100]* direction. This packing can be virtually separated into alternating layers formed by the chains of one particular type. Therefore, chains form two-layered packing with a distorted 2D pseudo-hexagonal motif (**Figure S8**). The packing is loose and contains cavities occupied by detaH$_2^{2+}$ cations and solvating H$_2$O and CH$_3$CN molecules. Carboxylic groups of tfa$^-$ anions, NH$_3$-groups of detaH$_2^{2+}$ cations and H$_2$O molecules form an extended framework of interchain hydrogen bonds (**Table S8**).

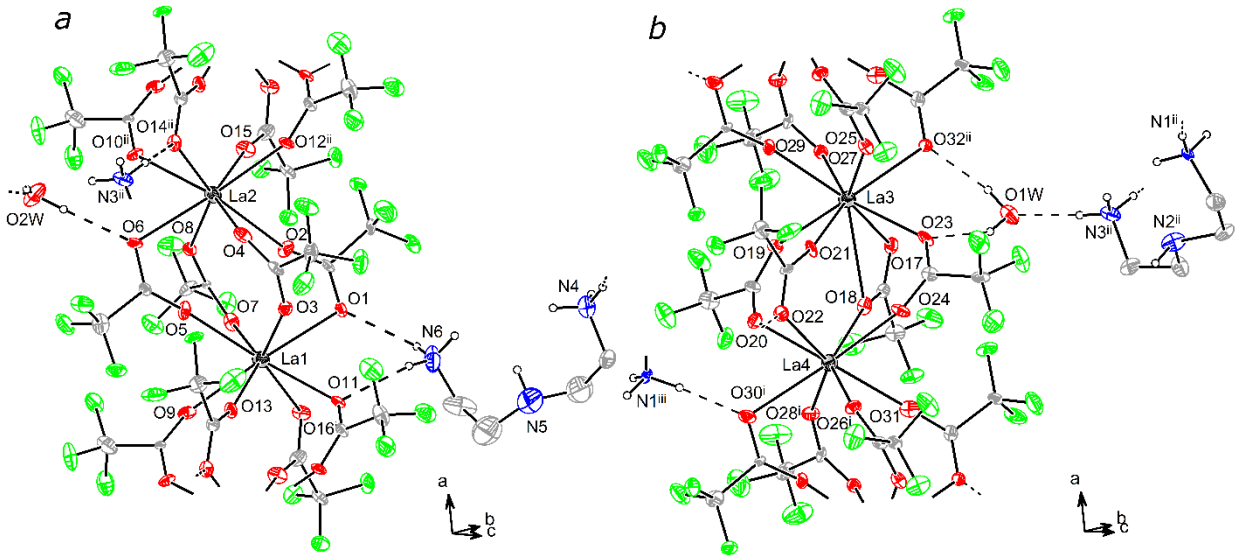

Figure S7. Fragments of anionic chains of first (a) and second (b) types in structure **1** with neighboring species. Hydrogen atoms are partially omitted for clarity. Dashed lines show intermolecular hydrogen bonds. Symmetry codes: (i) -1 + x, y, z, (ii) 1 + x, y, z, (iii) -x, -0.5+y, -z, (iv) 1 - x, -0.5 + y, 1 - z.

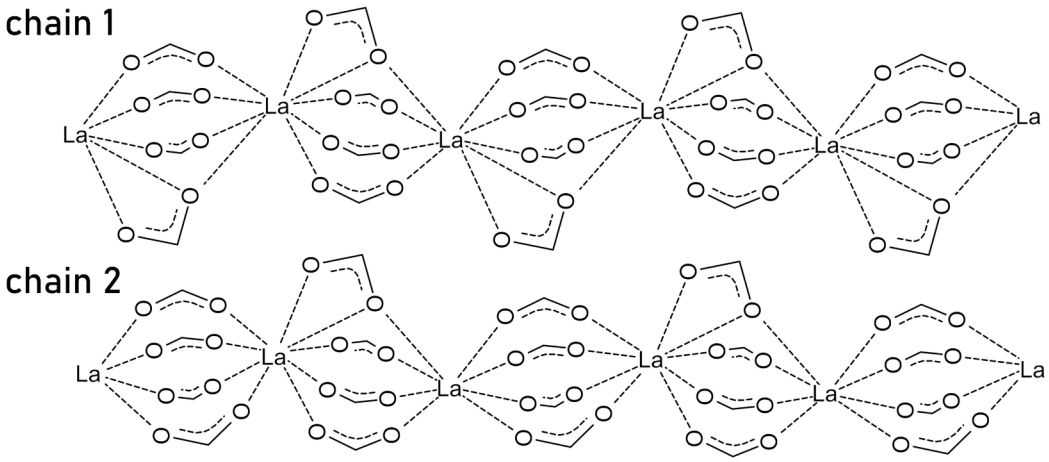

Scheme S1. Geometry of the polymeric chains of two types in the structure **1**. CF_3-groups are omitted.

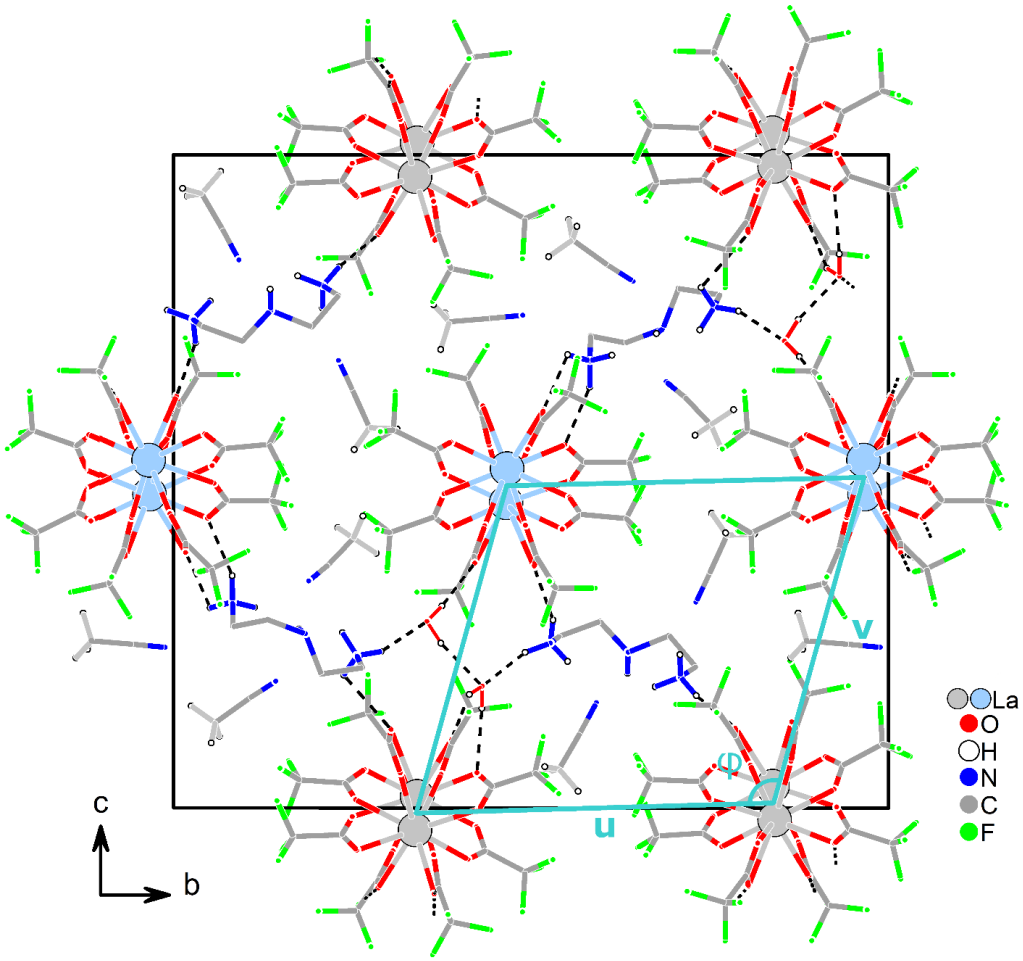

Figure S8. Two-layered packing of polymeric chains in the structure of $(detaH_2)_2[La_2(tfa)_8]_2(CH_3CN)_5(H_2O)_2\}_n$ (**1**). Light gray and light blue circles show La atoms within the chains of the first and the second types respectively. Hydrogen atoms are partially omitted for clarity. For disordered CF_3-groups the positions with major occupancy are depicted. Black solid lines show monoclinic unit cell edges, turquoise solid lines show pseudo-hexagonal 2D lattice based on ***u*** and ***v*** basis vector, $|\boldsymbol{u}|$ = 12.002(4) Å, $|\boldsymbol{v}|$ = 11.342(3) Å, φ = 107.143(4)°. Dashed lines show intermolecular hydrogen bonds.

Table S7. Interatomic distances (Å) in complex anions $[La_2(tfa)_8]^{2-}$ according to XRD data of $\{(detaH_2)_2[La_2(tfa)_8]_2 \cdot 5CH_3CN \cdot 2H_2O\}_n$ (**1**). Symmetry codes: (i) -1 + x, y, z, (ii) 1 + x, y, z.

La–L	d, Å	La–L	d, Å
La1–O1	2.595(17)	La3–O17	2.630(18)
La1–O3	2.502(17)	La3–O18	2.882(17)
La1–O5	2.483(16)	La3–O19	2.457(17)
La1–O7	2.512(17)	La3–O21	2.468(16)
La1–O9	2.524(19)	La3–O23	2.530(17)
La1–O11	2.559(17)	La3–O25	2.492(17)
La1–O13	2.530(17)	La3–O27	2.510(16)
La1–O16^{i}	2.553(18)	La3–O29	2.497(17)
La1–O2	3.033(17)	La3–O32^{ii}	2.560(17)
La2–O2	2.465(16)	La3–O18	2.882(17)
La2–O4	2.551(17)	La4–O18	2.532(16)
La2–O6	2.577(18)	La4–O20	2.500(17)
La2–O8	2.511(17)	La4–O22	2.539(18)
La2–O10^{ii}	2.526(16)	La4–O24	2.494(19)
La2–O12^{ii}	2.542(17)	La4–O26	2.450(18)
La2–O13^{ii}	2.995(17)	La4–O28	2.461(19)
La2–O14^{ii}	2.605(16)	La4–O30	2.626(17)
La2–O15	2.457(17)	La4–O31	2.455(18)
		La4–O29^{i}	3.164(17)
		La4–O21	3.083(17)

Table S8. Parameters of intramolecular hydrogen bonds O−H···O and N−H···O in structure **1**, (Å, °).

D−H	A	d(D−H)	d(H···A)	d(D_A)	∠DHA
N1−H1A	O30	0.909	1.950	2.85(3)	169.692
N3−H3A	O1W	0.910	1.849	2.73(3)	161.930
N3−H3C	O14	0.911	2.022	2.88(3)	154.668
N4−H4A	O2W	0.909	1.902	2.76(3)	155.637
N6−H6A	O1	0.910	2.297	2.76(3)	111.386
N6−H6B	O11	0.911	2.283	3.14(3)	156.689
O2W−H2WB	O6	0.857	2.089	2.94(3)	173.691
O2W−H2WA	O1W	0.866	1.999	2.85(3)	168.141
O1W−H1WA	O23	0.872	2.167	2.97(3)	153.190
O1W−H1WB	O32	0.878	2.042	2.84(3)	150.984

*2.3. Crystal Structure of $(detaH_2)_n[Ln_2(tfa)_8]_n$, Ln = Pr(**2**), Nd(**3**), Sm (**4**), and Eu (**5**).*

According to single crystal XRD data for **2**-**3** and PXRD data for **2**-**5**, these compounds are isostructural, and therefore only **3** will be discussed as an example. The asymmetric part of orthorhombic unit cell contains two anionic chains $[Nd(tfa)_4]_n^{n-}$ and one cationic species $detaH_2^{2+}$ (**Figure S9**). Anionic chains of the first type contain Nd1 atoms, while the ones of the second types contain Nd2 atoms. Coordination environment of Nd1 and Nd2 differs in details despite similar polyhedron (CN = 8, square antiprism, CShM = 1.312 and 0.044 respectively, Table S3). Namely, Nd1 is coordinated by O1 and O2 atoms of a κ^2-carboxylate group (Nd1–O1 and Nd1–O2 distance 2.596(6) and 2.586(5) Å respectively, Table S10), and O3, $O4^{ii}$, O5, $O6^{i}$, O7 and O8 atoms (mean Nd1–O distance 2.45(3) Å) of six distinct μ^2-κ^1:κ^1-carboxylate groups. Nd2 is coordinated by O9, $O10^{v}$, $O11^{iv}$, O12, O13, O14, $O15^{iv}$ and O16 atoms (mean Nd2–O distance 2.446(17) Å) of the eight μ^2-κ^1:κ^1-carboxylate groups (**Table S9**).

The chains of both types are packed parallel to neighbors along *[001]* direction through the interchain hydrogen bonds (**Table S10**). This packing can be virtually separated into alternating layers formed by the chains of only one type. Therefore, chains form two-layered packing with a distorted 2D pseudo-hexagonal motif (**Figure S10**).

The packing is tighter than in structure of **1** (as monitored by 2D lattice parameters ***u*** and ***v***, **Table S12**) and the packing cavities are occupied only by $detaH_2^{2+}$ cations with no solvent molecules. Carboxylic groups of tfa^- anions and NH_3-groups of $detaH_2^{2+}$ cations form an extended framework of interchain hydrogen bonds (**Table S10**). Comparison of structures **2** and **3** reveals the inhomogeneous changes of Ln – O and hydrogen bond lengths (**Table S9**, **S10**) caused by decrease of ionic radius of Ln from Pr to Nd and slight rearrangement of entire chains (shortening of ***v*** and elongation of ***u*** parameters of pseudo-hexagonal packing, **Table S11**). According PXRD data the unit cell parameters of **2-5** decrease along with reduction of ionic radius from Pr to Eu (**Table S12**). Some examples of polymeric REE *tetrakis*-trifluoroacetates were described in previous works [3-6]. Moreover, similar diatomic fragments with four bridging tfa^- anions have been observed before [7-10]. Nevertheless, the complexes **1**-**5** are the first examples of *tetrakis*-trifluoroacetates with anionic chain with chelating carboxylate groups.

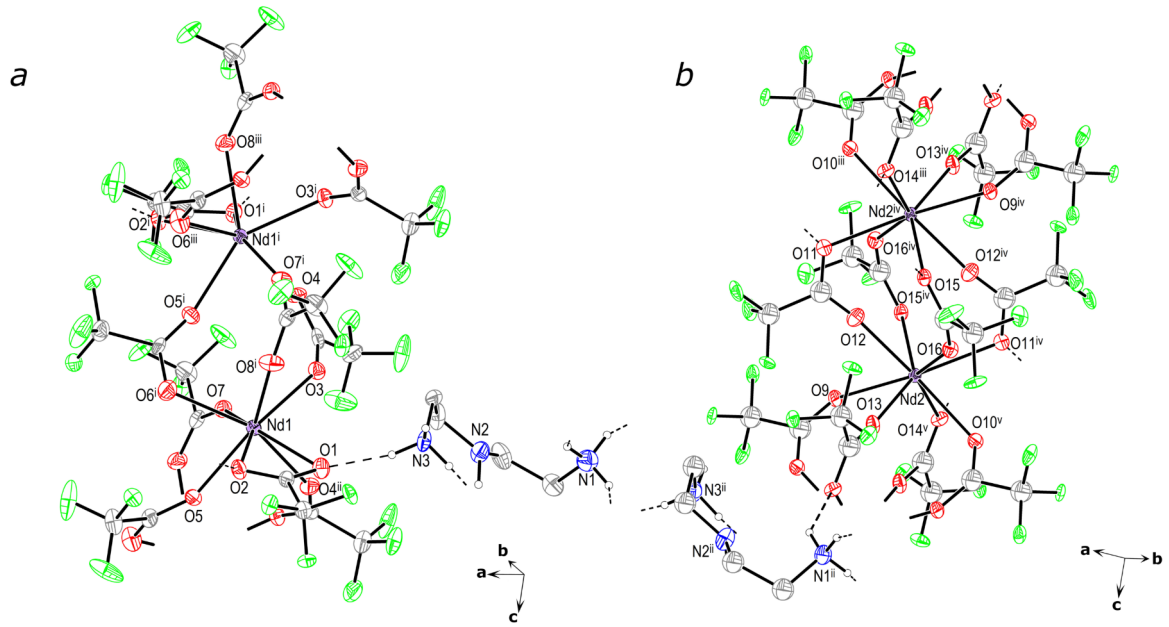

Figure S9. Selected fragments of structure **3**: anionic chains $[Nd(tfa)_4]^-$ containing Nd1 (*a*) or Nd2 (*b*) atoms with neighbouring cationic species $detaH_2^{2+}$. Symmetry codes: (i) -0.5 + x, y, 0.5 – z, (ii) 0.5 + x, y, 0.5 – z, (iii) -1 + x, y, z, (iv) 2 – x, 1 – y, 1 – z, (v) 3 – x, 1 – y, 1 – z. Hydrogen atoms are partially omitted for clarity. Dashed lines show the hydrogen bonds.

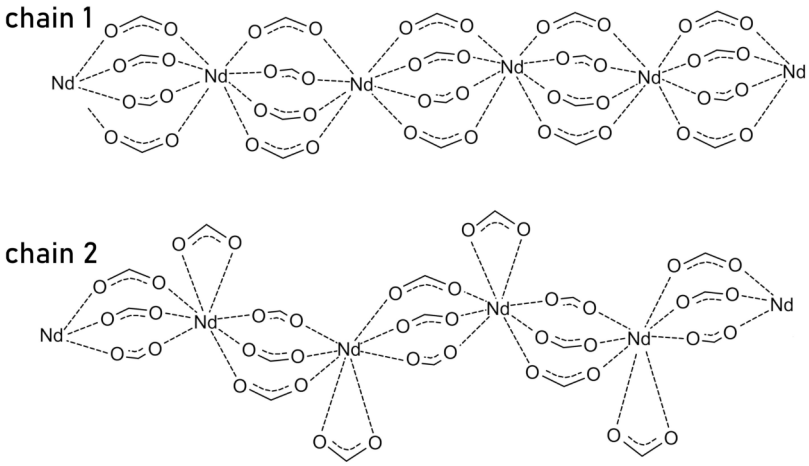

Scheme S2. Geometry of the polymeric chains of two types in the structure **1**. CF_3-groups are omitted.

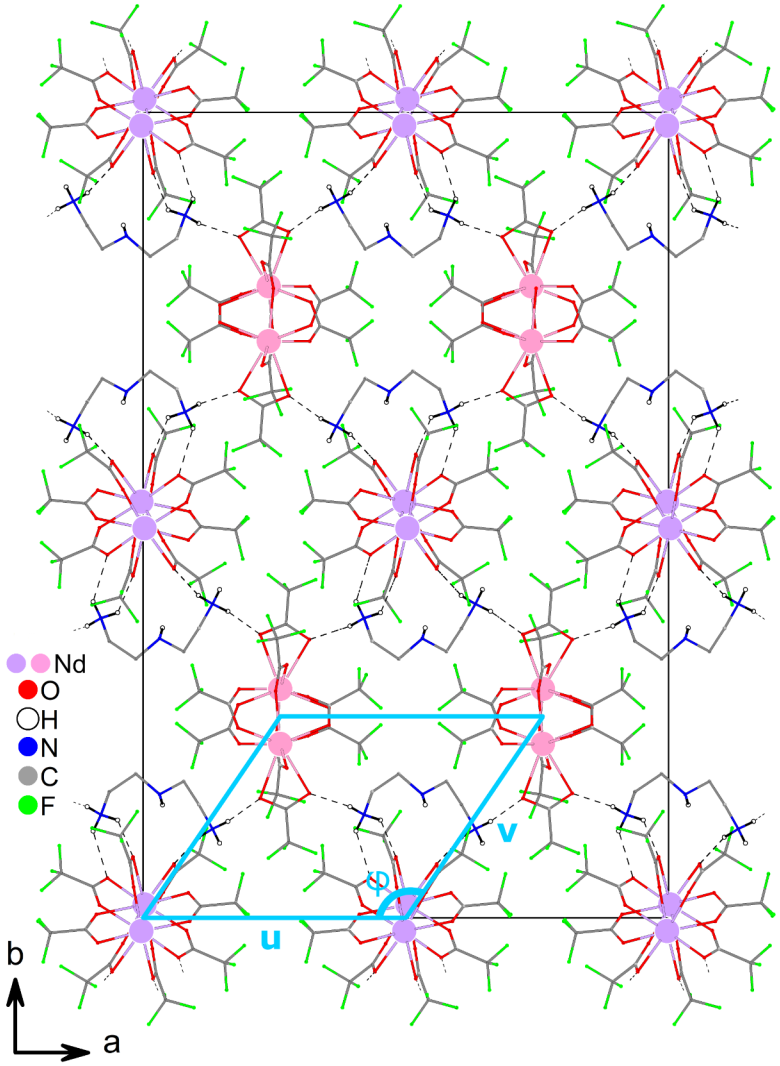

Figure S10. Two-layered packing motif of polymeric chains in the structure of $(detaH_2)_n[Nd_2(tfa)_8]_n$ (**3**). Black lines show unit cell edges, blue lines show pseudo-hexagonal 2D lattice based on **u** and **v** basis vector, |**u**| = 11.725(3) Å, |**v**| = 10.5786(14) Å, φ = 122.012(2)˚. Hydrogen atoms are partially omitted for clarity. Dashed lines show intermolecular hydrogen bonds.

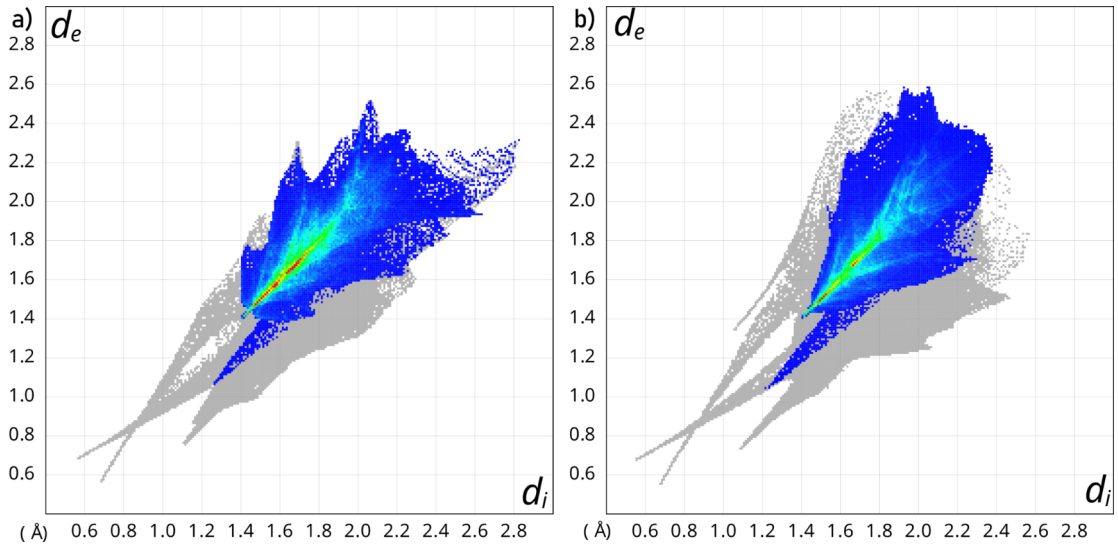

Figure S11. Hirshfield surface fingerprint plots [11] for chain with bridging (a) and chelato-bridging (b) ligands in structure **3**. Partial atomic contribution to intermolecular interactions are F···F 54.4%, F···H 21.6%, O···H 12.6% (a) and F···F 43.5%, F···H 33.8%, O···H 12.9% (b).

Table S9. Interatomic distances (Å) in complex anions $[Ln(tfa)_4]^-$ according to XRD data of **2-3**. Symmetry codes: (i) -0.5 + x, y, 0.5 – z, (ii) 0.5 + x, y, 0.5 – z, (iv) 2 – x, 1 – y, 1 – z, (v) 3 – x, 1 – y, 1 – z, (vi) -1 + x, y, z.

Ln–L	Ln = Pr (**2**)	Ln = Nd (**3**)
Ln1–O1	2.610(14)	2.594(5)
Ln1–O2	2.573(14)	2.583(5)
Ln1–O3	2.439(14)	2.394(5)
Ln1–O4^{ii}	2.441(13)	2.427(5)
Ln1–O5	2.419(13)	2.395(5)
Ln1–O6^{i}	2.367(13)	2.440(7)
Ln1–O7	2.415(13)	2.391(6)
Ln1–O8^{i}	2.408(15)	2.423(6)
Ln2–O9	2.416(14)	2.432(5)
Ln2–O10^{v}	2.463(13)	2.453(5)
Ln2–O11^{iv}	2.526(11)	2.531(5)
Ln2–O12	2.417(14)	2.406(5)
Ln2–O13	2.398(14)	2.387(5)
Ln2–O14^{v}	2.502(14)	2.508(5)
Ln2–O15^{iv}	2.495(14)	2.478(5)
Ln2–O16	2.431(14)	2.438(5)

Table S10. Parameters of intramolecular hydrogen bonds O−H···O and N−H···O in complexes **2**-**3** (Å, °).

D−H	A	d(D−H)	d(H···A)	d(D_A)	∠DHA
Ln = Pr (**2**)					
N1−H1A	O15	0.911	2.481	3.03(2)	119.495
N1−H1B	O14	0.910	2.138	2.81(2)	145.881
N1−H1C	O2	0.910	2.139	2.87(2)	136.258
N3−H3B	O11	0.909	1.943	2.83(2)	165.952
N3−H3C	O1	0.911	1.945	2.83(2)	164.426
Ln = Nd (**3**)					
N1−H1A	O15	0.910	2.305	3.05(8)	138.851
N1−H1B	O14	0.910	2.007	2.82(8)	138.419
N1−H1C	O2	0.910	1.995	2.88(9)	155.350
N3−H3B	O11	0.907	1.966	2.86(8)	168.818
N3−H3C	O1	0.911	1.918	2.81(9)	166.402

Table S11. Pseudo-hexagonal unit cell parameters for complexes **1**-**3** estimated from the full-profile refinement of PXRD data.

Ln	La (**1**)	Pr (**2**)	Nd (**3**)
U	12.002(4) Å	11.669(8) Å	11.725(3) Å
V	11.342(3)Å	10.861(5) Å	10.5786(14) Å
Φ	107.143(4)˚	124.129(6)˚	122.012(2)˚

Table S12. Orthorombic unit cell parameters for complexes **2**-**5** estimated from the full-profile refinement of PXRD data at 300K.

Ln	Pr (**2**)	Nd (**3**)	Sm (**4**)	Eu (**5**)
a, Å	8.83(11)	8.78(11)	8.755(03)	8.667(02)
b, Å	23.80(04)	23.78(04)	23.731(08)	23.455(04)
c, Å	36.44(03)	36.34(03)	36.229(11)	35.949(10)

*2.4. Crystal Structure of $[La(tfa)_3(CH_3CN)(H_2O)]_n$ (**6**).*

The asymmetric part of monoclinic unit cell of **6** contains La1 atom, three tfa^- anions, and one CH_3CN and one H_2O ligands (**Figure S12**). Coordination environment of La1 complies with biaugmented trigonal prism (CShM = 1.135, CN = 8, Table S4). La1 atom is coordinated by $O1^i$, O2, O3, $O4^{ii}$, O5, $O6^{ii}$ of the three μ^2-κ^1:κ^1-carboxylate groups (mean La1–O distance 2.50(2) Å, Table S14), O1W atom of water molecule and N1 atom of CH_3CN molecule. Additionally, weak elongated contact La1···O1 (3.010(2) Å) reveals one carboxylate group with slightly expressed chelate-bridging coordination. The latter causes the formation of centrosymmetric dimeric species $[La_2(tfa)_6(CH_3CN)_2(H_2O)_2]$ with the shortest La1···$La1^i$ distance being equal to 4.6528(5) Å (**Table S13**).

Dimeric species are assembled into polymeric layers with pseudo-hexagonal packing motif via bridging tfa^- anions and interdimeric hydrogen bonds (Table S14). It is worth noting that interdimeric La···La distances (5.6486(5) Å) are significantly larger than intradimeric one. Layers are packed parallel to *(011)* plane, and CF_3-groups of tfa^- anions and CH_3-groups of CH_3CN are directed into the interlayer space (**Figures S13**, **S14**).

Therefore, complex **6** is a rare example of lanthanide trifluoroacetate complex with 2D polymeric structure which contained coordinated solvent molecules, while previously reported ones, either with coordinated or external solvent molecules, demonstrate 1D polymeric structure [12-16].

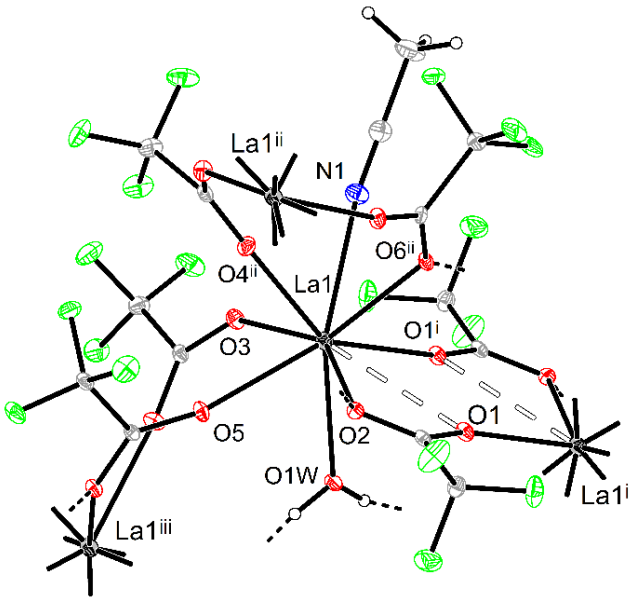

Figure S12. Selected fragments of structure **6**. Symmetry codes: (i) 1 – x, 1 – y, 1 – z, (ii) x, 0.5 – y, -0.5 + z, (iii) x, 0.5 – y, 0.5 + z. Black dashed lines show the hydrogen bonds. Empty dashed lines show the elongated La1···O1 contacts.

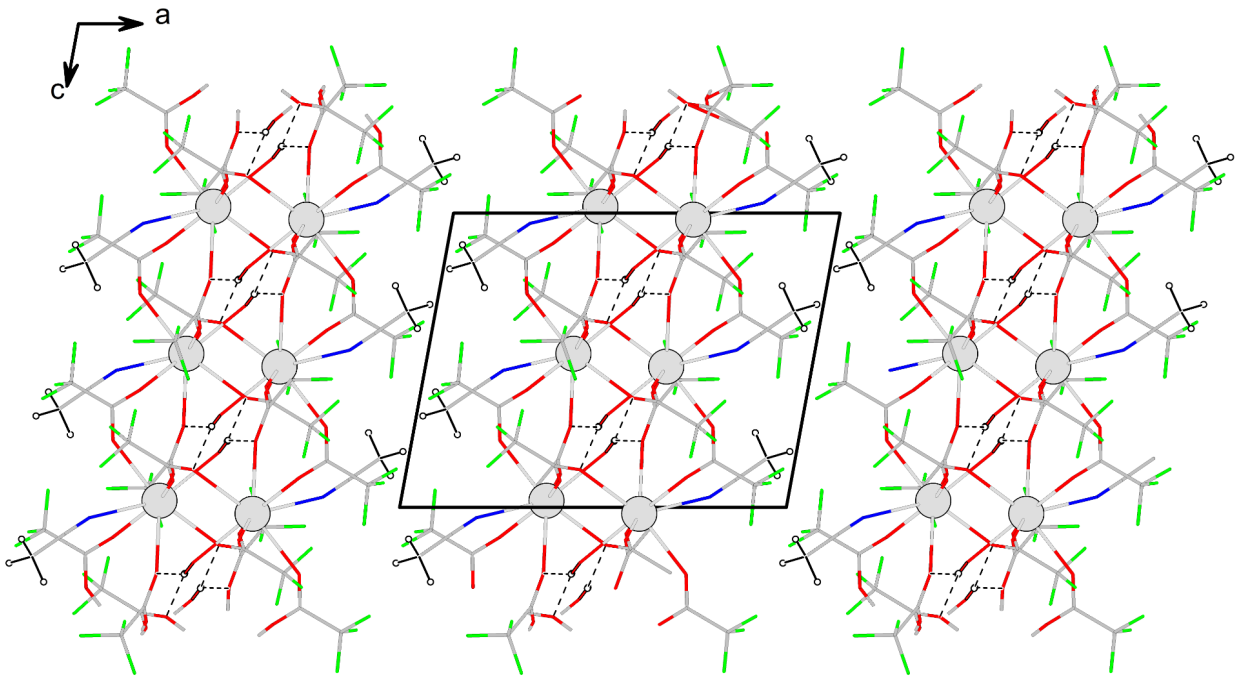

Figure S13. Packing of polymeric layers within the structure of $[La(tfa)_3(CH_3CN)(H_2O)]_n$ (**6**). Black lines show unit cell edges. Dashed lines show intermolecular hydrogen bonds within the layers.

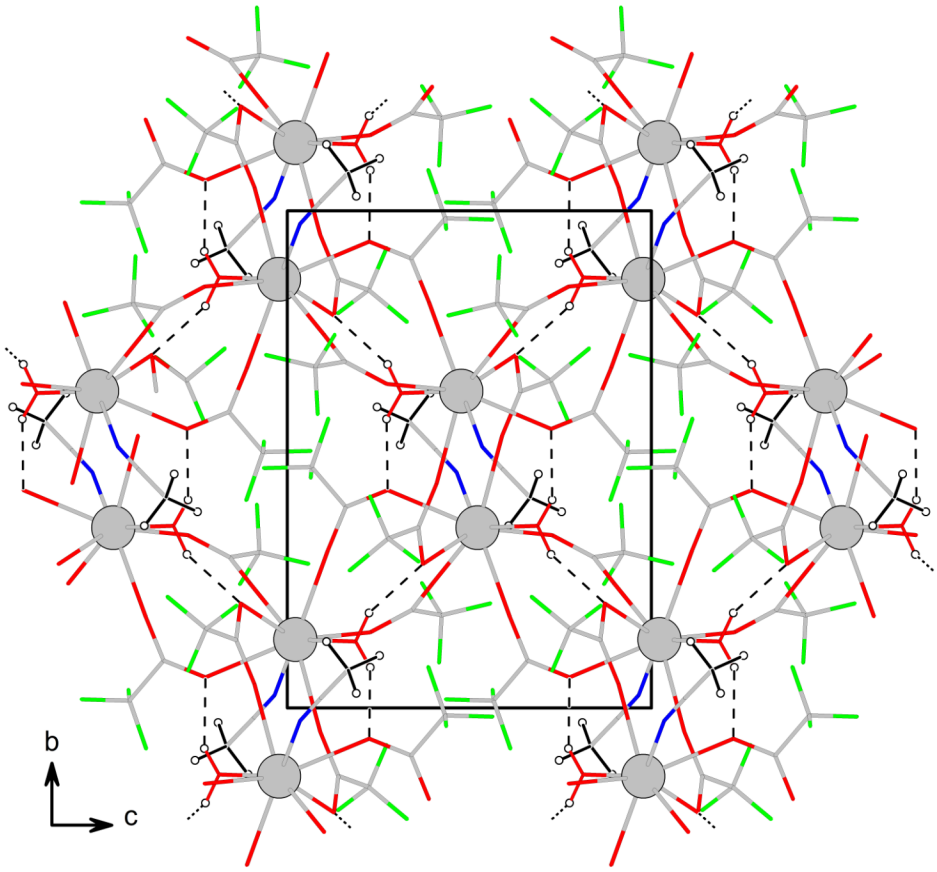

Figure S14. The structure of pseudo-hexagonal layer in $[La(tfa)_3(CH_3CN)(H_2O)]_n$ (**6**). The orientation of the coordinate system along the axis ***a***. Black lines show unit cell edges. Dashed lines show intermolecular hydrogen bonds in the layers.

Table S13. Interatomic distances (Å) in complex **6** according to XRD data. Symmetry codes: (i) 1 – x, 1 – y, 1 – z, (ii) x, 0.5 – y, -0.5 + z.

La–L	d, Å
La–O1^{i}	2.506(2)
La–O2	2.5739(19)
La–O3	2.474(2)
La–O4^{ii}	2.406(2)
La–O5	2.485(2)
La–O6^{ii}	2.554(2)
La–O1W	2.481(2)
La–N1	2.737(3)

Table S14. Parameters of intramolecular hydrogen bonds O−H···O in complex **6**, (Å, °).

D−H	A	d(D−H)	d(H···A)	d(D_A)	∠DHA
O1W−H1W	O2	0.862	1.984	2.805(3)	158.731
O1W−H2W	O6	0.825	2.045	2.797(3)	151.406

*2.5. Crystal Structure of [Gd(tfa)$_3$(deta)$_2$](^{i}PrOH) (**7**).*

The asymmetric part of monoclinic unit cell of **7** contains one mononuclear [Gd(tfa)$_3$(deta)$_2$] molecule (**Figure S15**) and one ^{i}PrOH solvent molecule. Within [Gd(tfa)$_3$(deta)$_2$] molecule Gd1 atom being in spherical capped square antiprismatic coordination environment (CShM = 0.664, CN = 9, **Table S5**) is coordinated by O1, O3 and O5 atoms (mean Gd1–O distance 2.395(12) Å, Table S15) of a κ^1-carboxylate groups of three terminal tfa$^-$ anions and six N1-N6 atoms of two chelating deta ligands (mean Gd1–N distance 2.573(6) Å, **Table S15**). Uncoordinated O-atoms of tfa$^-$ ligands, O2, O4, O6, form the framework of intermolecular hydrogen bonds with NH$_2$-groups of deta ligands that causes the association of neighboring molecules into layers parallel to *(011)* plane (**Table S16**, **Figure S16-S17**). Within the layers there are the packing cavities occupied by ^{i}PrOH molecules. The later was localized from difference Fourier synthesis but the refinement was unstable due to disordering and poor crystal qualities. The best results of data refinement were obtained after solvent elimination by SQUEEZE-procedure. The formation and geometry of [Ln(tfa)$_3$(deta)$_2$] molecules for Tb and lighter REE have been predicted by DFT calculations [17] but **7** is the first obtained example of the series.

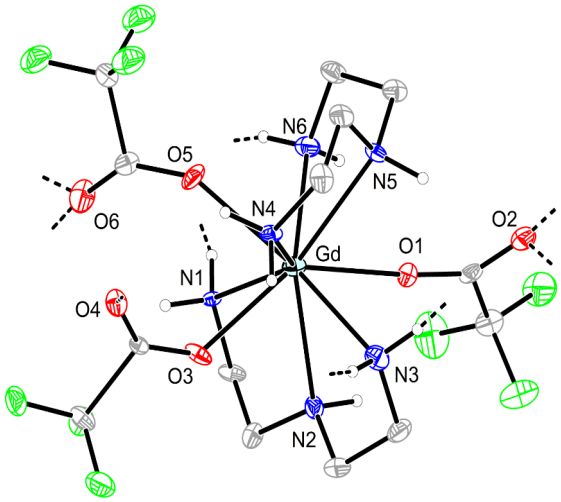

Figure S15. Molecular geometry [Gd(tfa)$_3$(deta)$_2$] in structure **7**. Hydrogen atoms are partially omitted for clarity. Dashed lines show intermolecular hydrogen bonds.

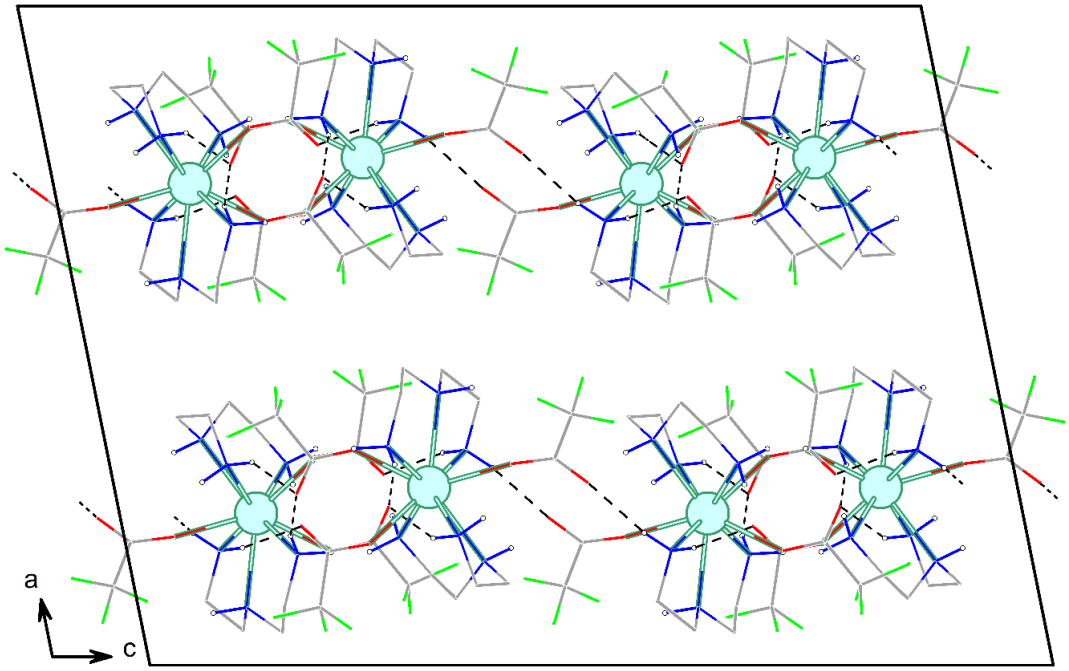

Figure S16. Packing of $[Gd(tfa)_3(deta)_2]$ molecules within the structure **7**. Hydrogen atoms are partially omitted for clarity, ^{i}PrOH molecules were squeezed. Black lines show unit cell edges. Dashed lines show intermolecular hydrogen bonds within the H-bonded layers.

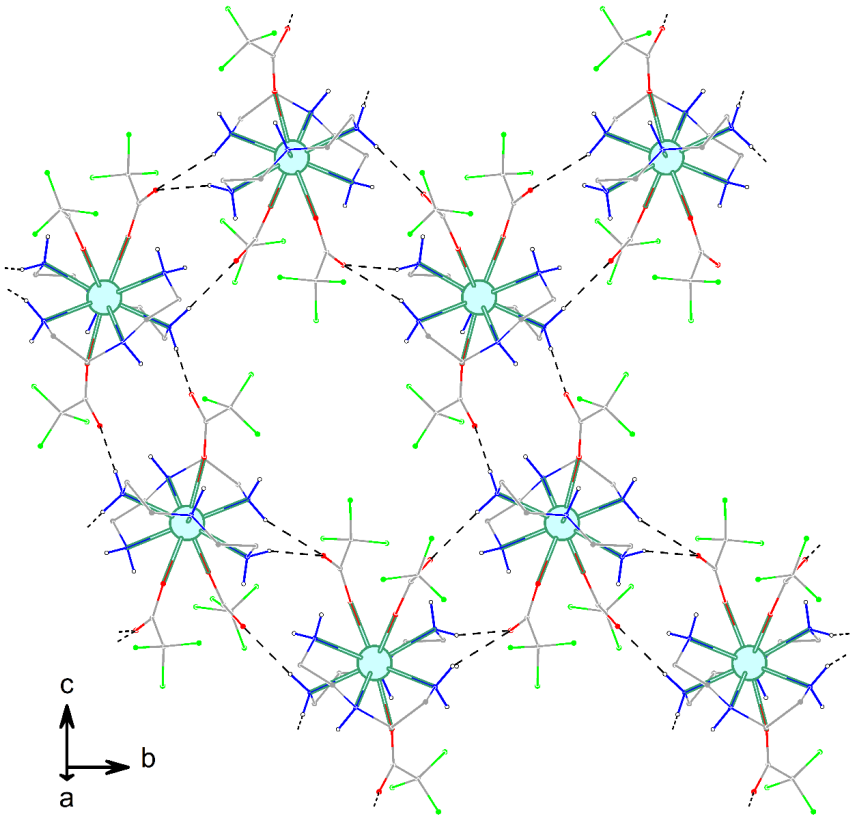

Figure S17. Fragment of H-bonded layer in the structure **7**. Hydrogen atoms are partially omitted for clarity. Dashed lines show intermolecular hydrogen bonds in the layers.

Table S15. Interatomic distances (Å) in complex **7** according to XRD data.

Gd–L	d, Å
Gd–O1	2.399(10)
Gd–O3	2.394(13)
Gd–O5	2.372(11)
Gd–N1	2.570(13)
Gd–N2	2.580(14)
Gd–N3	2.563(14)
Gd–N4	2.575(14)
Gd–N5	2.623(16)
Gd–N6	2.554(18)

Table S16. Parameters of intramolecular hydrogen bonds N−H···O in complex **7**, (Å, °).

D−H	A	d(D−H)	d(H···A)	d(D_A)	∠DHA
N1−H1B	O4	0.910	2.192	3.07(3)	161.946
N3−H3A	O2	0.910	2.112	3.02(2)	172.453
N3−H3B	O6	0.910	2.350	3.25(2)	168.789
N6−H6B	O4A	0.910	2.108	2.96(3)	155.055

*2.6. Crystal Structure of [Yb(tfa)$_2$(deta)$_2$](tfa) (**8**).*

The complex **8** is isostructural to [Y(tfa)$_2$(deta)$_2$](tfa) analog reported by us earlier [17]. The asymmetric part of monoclinic unit cell of complex **8** contains [Yb(tfa)$_2$(deta)$_2$]$^+$ complex cation and outer-sphere tfa$^-$ anion (**Figure S18**). The Yb1 coordination geometry is best be described as triangular dodecahedron (CShM = 0.978, CN = 8, **Table S6**). The Yb1 is coordinated by O1 and O3 atoms (mean Yb1–O distance 2.250(2) Å, **Table S17**) of a κ^1-carboxylate groups of two terminal tfa$^-$ anions and six atoms N1-N6 of two chelating deta ligands (mean Yb1–N distance 2.479(2) Å, **Table S17**). It worth noting, that Ln–O and Ln–N in **8** are shorter than ones in yttrium analog (mean Ln–O and Ln–N distance are equal to 2.276(17) Å and 2.531(6) Å respectively) due to smaller ionic radius of Yb [18]. The formation of dimeric units with hydrogen bonds (Table S18) and packing features were discussed earlier for isostructural complexes [17].

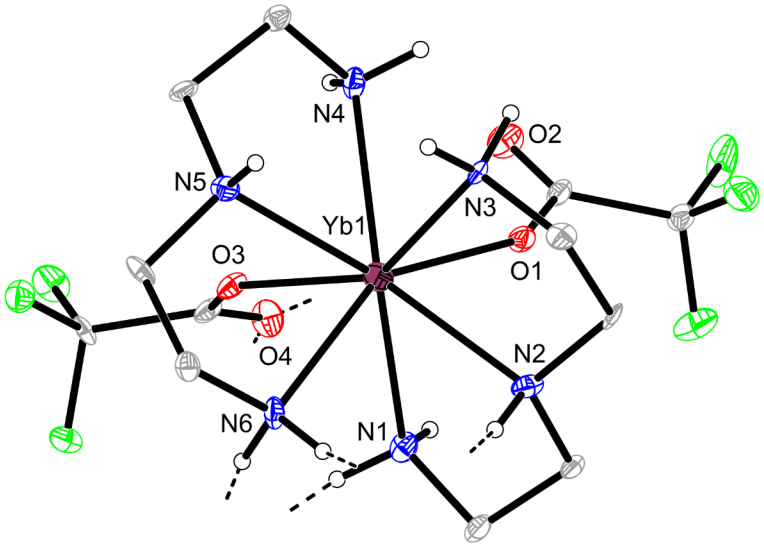

Figure S18. Complex fragment [Yb(tfa)$_2$(deta)$_2$]$^-$ of structure **8**. Hydrogen atoms are partially omitted for clarity. Dashed lines show intermolecular hydrogen bonds.

Table S17. Interatomic distances (Å) in complex **8** according to XRD data.

Yb–L	d, Å
Yb –O1	2.229(8)
Yb –O3	2.258(7)
Yb –N1	2.453(9)
Yb –N2	2.482(8)
Yb –N3	2.512(9)
Yb –N4	2.497(9)
Yb –N5	2.504(9)
Yb –N6	2.472(7)

Table S18. Parameters of intramolecular hydrogen bonds N–H···O in complexes **8**, (Å, °).

D–H	A	d(D–H)	d(H···A)	d(D_A)	∠DHA
N1–H1A	O4	0.911	2.181	3.024(12)	153.526
N3–H3A	O6	0.911	2.168	3.079(13)	166.508
N3–H3B	O6	0.910	2.146	3.040(12)	167.152
N6–H6A	O4	0.910	2.106	3.007(12)	170.371
N6–H6B	O5	0.910	2.160	3.031(12)	159.976

*2.7. Crystal Structure of (detaH$_2$)(tfa)$_2$ (**9**).*

The asymmetric part of triclinic unit cell of **9** contains two double protonated detaH$_2^{2+}$ cations and four tfa$^-$ anions. Each NH$_3$-group of detaH$_2^{2+}$ forms three hydrogen bonds with carboxylic groups of tfa$^-$ anions, while NH-groups do not participate in hydrogen bonds. The framework of hydrogen bonds leads to assembly of cationic and anionic species into layers which are packed parallel to (*011*) plane (**Table S19**, **Figure S19-S20**). CF$_3$-groups are directed into interlayer space.

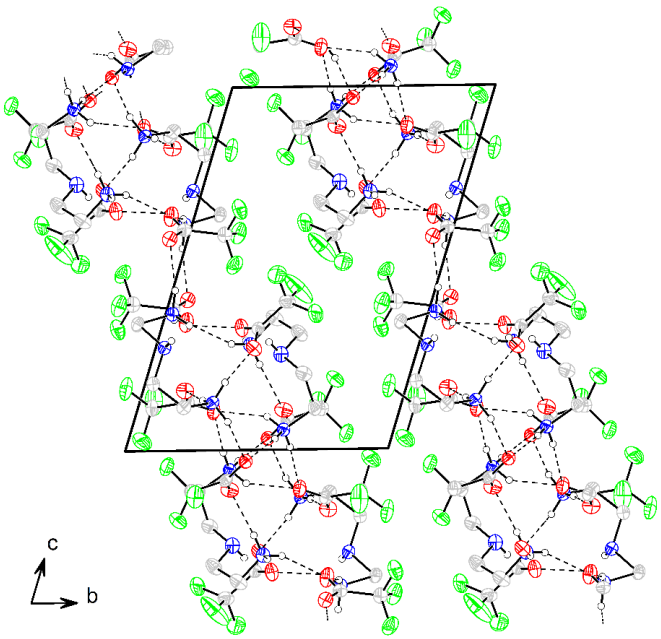

Figure S19. Monoclinic packing in the structure of (detaH$_2$)(tfa)$_2$ (**9**). Black lines show unit cell edges. Dashed lines show intermolecular hydrogen bonds in the layers.

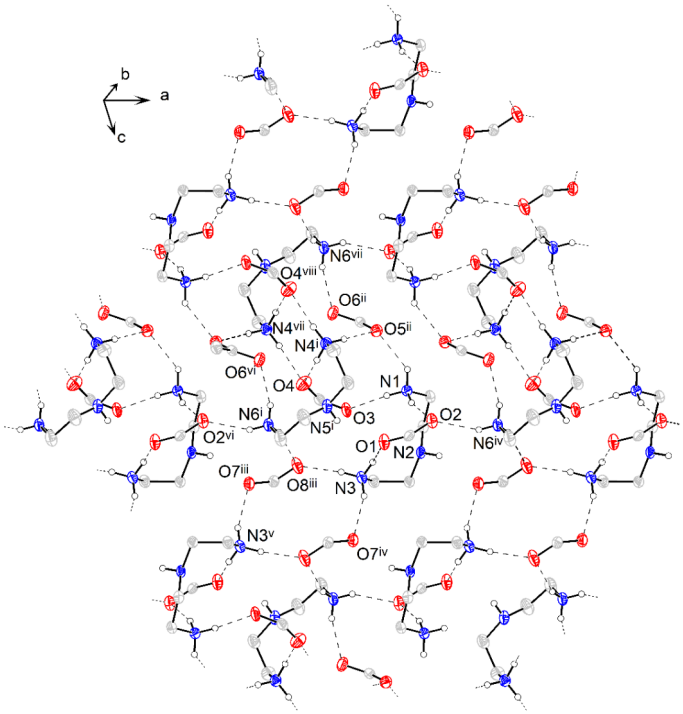

Figure S20. The structure of layer in the structure of (detaH$_2$)(tfa)$_2$ (**9**). Dashed lines show intermolecular hydrogen bonds in the layers. The trifluoroacetate groups are emitted.

Table S19. Parameters of intramolecular hydrogen bonds N−H···O in complex **9**, (Å, °).

D−H	A	d(D−H)	d(H···A)	d(D_A)	∠DHA
N1−H11	O3	0.934	1.895	2.825(4)	173.072
N1−H12	O5	0.934	2.121	2.884(3)	137.966
N1−H13	O2	0.934	1.918	2.826(5)	163.505
N−H31	O7	0.913	2.034	2.896(3)	156.708
N−H32	O8	0.913	1.930	2.822(3)	165.254
N−H33	O1	0.913	2.046	2.854(4)	146.738
N4−H41	O5	0.896	1.986	2.865(3)	166.123
N4−H42	O4	0.896	2.123	2.919(4)	147.457
N4−H43	O4	0.898	1.946	2.838(4)	172.183
N6−H61	O8	0.840	2.066	2.859(3)	157.305
N6−H62	O2	0.838	2.045	2.814(4)	152.313
N6−H63	O6	0.837	2.019	2.824(3)	161.296

3. Thermal behavior and TGA data.

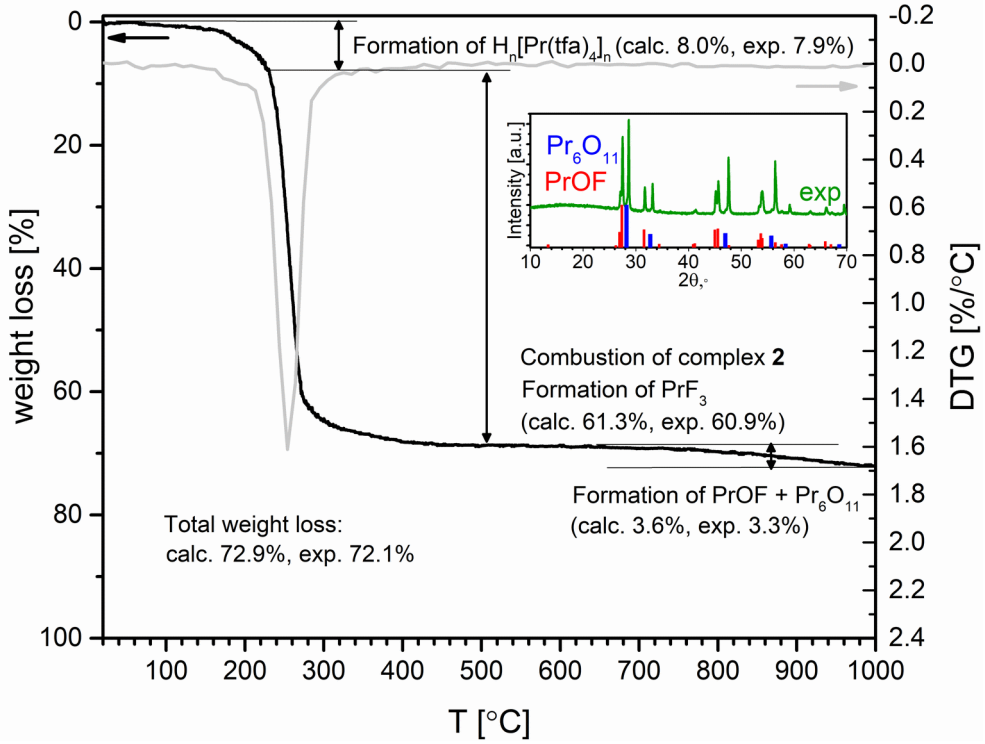

Figure S21. The data of TGA on the thermal behavior of **2** upon heating in air. The black line shows the TG curve, pale grey line shows the DTG curve, the insert presents the PXRD of the residue compared to cards [44-1312] for PrOF and [42-1121] for Pr_6O_{11} from PDF-2 data base upon λ = 1.5418 Å.

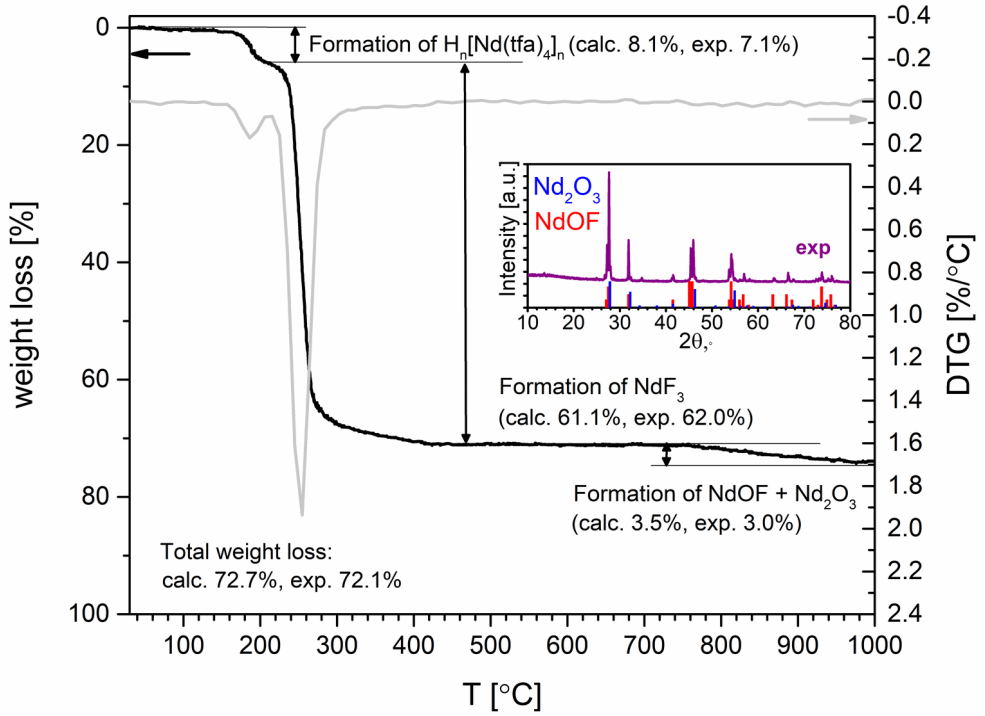

Figure S22. The data of TGA on the thermal behavior of **3** upon heating in air. The black line shows the TG curve, pale grey line shows the DTG curve, the insert presents the PXRD of the residue compared to cards [17-276] for NdOF and [21-579] for Nd_2O_3 from PDF-2 data base upon λ = 1.5418 Å.

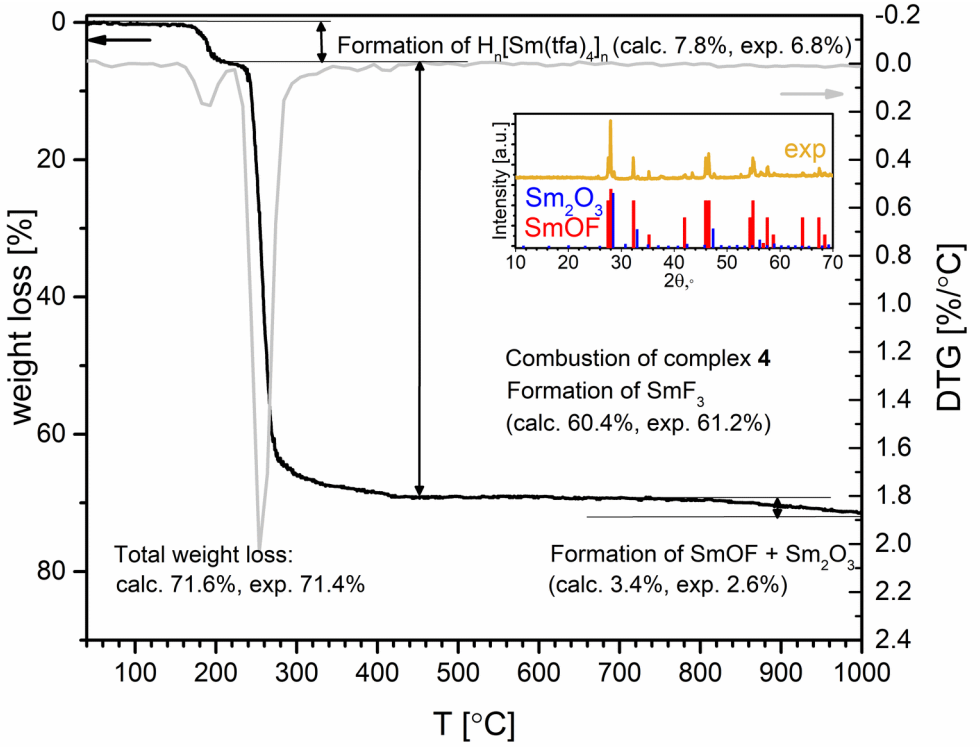

Figure S23. The data of TGA on the thermal behavior of **4** upon heating in air. The black line shows the TG curve, pale grey line shows the DTG curve, the insert presents the PXRD of the residue compared to cards [24-846] for SmOF and [74-1989] for Sm_2O_3 from PDF-2 data base upon λ = 1.5418 Å.

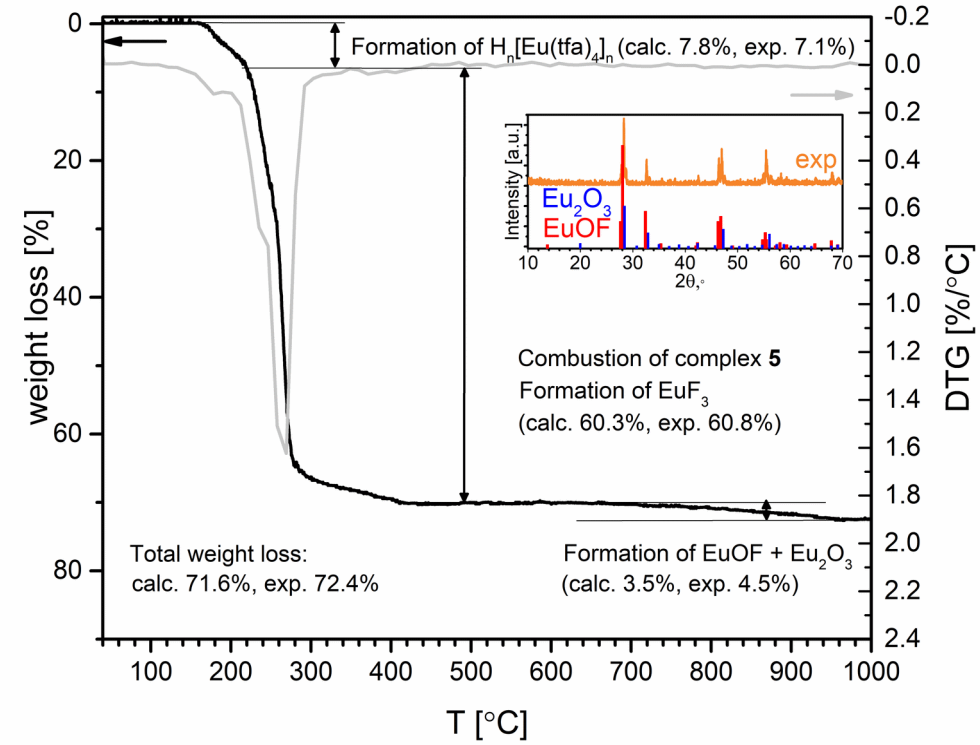

Figure S24. The data of TGA on the thermal behavior of **5** upon heating in air. The black line shows the TG curve, pale grey line shows the DTG curve, the insert presents the PXRD of the residue compared to cards [26-636] for EuOF and [34-392] for Eu_2O_3 from PDF-2 data base upon λ = 1.5418 Å.

4. EDX data for β-$NaGdF_4$: Yb, Er, Nd film.

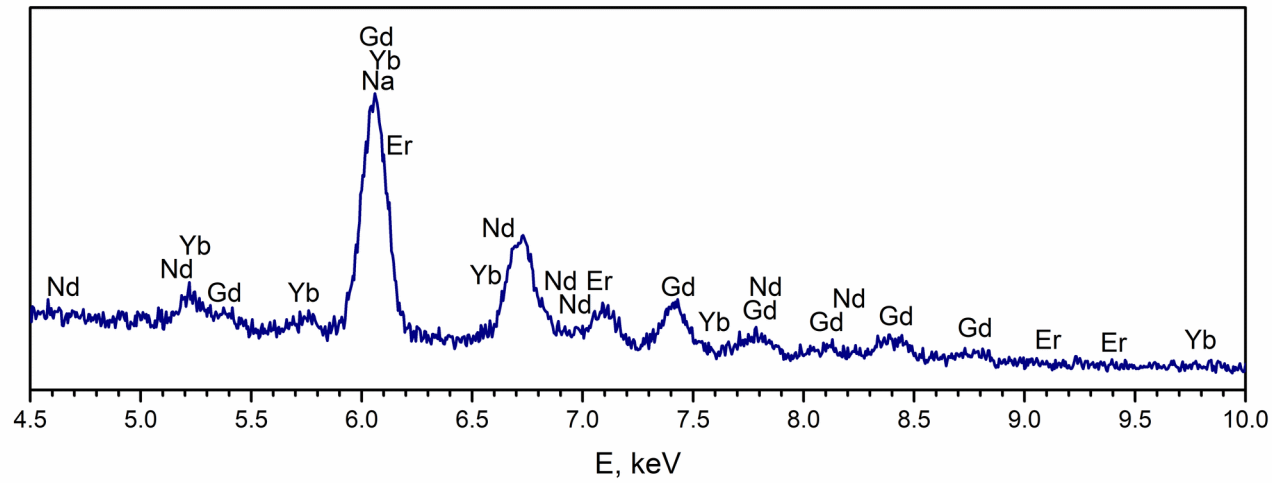

Figure S25. EDX spectrum of β-$NaLnF_4$//Al_2O_3 thin film. Elemental composition of film according to EDX is 70.2% of Gd, 6.4% of Nd, 2.7% of Er and 20.7% of Yb.

5. AFM data for β-$NaGdF_4$: Yb, Er, Nd film.

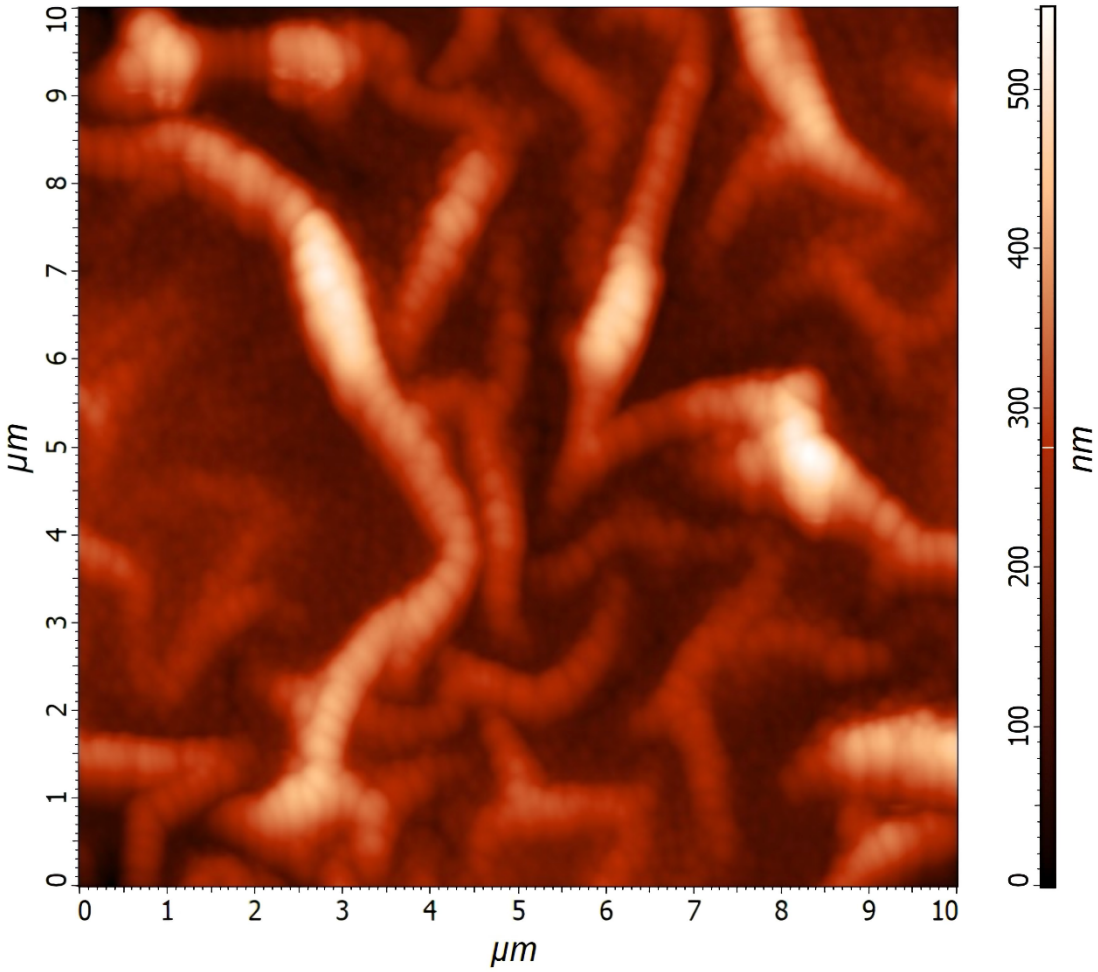

Figure S26. AFM height profiles of β-$NaLnF_4$//Al_2O_3 thin film. The film which is obtained from gel with deta has a clearly folded surface.

References

1 D. Grebenyuk, M. Zobel, M. Polentarutti, L. Ungur, M. Kendin, K. Zakharov, P. Degtyarenko, A. Vasiliev and D. Tsymbarenko, *Inorg. Chem.*, 2021, **60**(11), 8049.
2 A. Spek, *Acta Cryst.* 2020, **E76**, 1.
3 D. Grebenyuk, I. Martynova and D. Tsymbarenko, *Eur. J. Inorg. Chem*., 2019, 26, 3103.
4 D. Tsymbarenko, D. Grebenyuk, M. Burlakova and M. Zobel, *J. Appl. Cryst*., 2022, 55, 890.
5 M. Burlakova, M. Shaulskaya, A. Anosov and D. Tsymbarenko, *J. Struct. Chem*., 2023, **64**, 112528.
6 D. Tsymbarenko, D. Grebenyuk, M. Burlakova and A. Shurkina, *Russ. J. Coord. Chem*., 2022, **48**, 168.
7 S. Bone, D. Sowerby and R. Verma, *Dalton Trans*., 1978, 1544.
8 N. Dong, H. Wang, R. Barton and B. Robertson, *J. Coord. Chem*., 1990, **22**, 191.
9 P.-R. Wei, D.-D. Wu, Zh.-Yu. Zhou, S.-L. Li and T. C. W. Mak, *Polyhedron,* 1997, **16**, 749.
10 H. Ayadi, W. Fang, Sh. Mishra, E. Jeanneau, G. Ledoux, J. Zhang and S. Daniele, *RSC Adv*., 2015, **5**, 100535.
11 P. Spackman, M. Turner, J. McKinnon, S. Wolff, D. Grimwood, D. Jayatilakab and M. Spackman, *J. Appl. Cryst*., 2021, **54**, 1006.
12 S. Gutnikov, E. Karpova, M. Zakharov and A. Boltalin, *Russ. J. Inorg. Chem.*, 2006, **51**, 541.
13 B. Purohit, E. Jeanneau, Th. Cornier, G. Ledoux and Sh. Mishra, *J. Indian Chem. Soc.,* 2022, **99**, 100322.
14 Sh. Mishra, L. Hubert-Pfalzgraf, S. Daniele, M. Rolland, E. Jeanneau and B. Jouguet, *Inorg. Chem. Comm.*, 2009, 12, 97.
15 B. Purohit, E. Jeanneau, Y. Guyot, D. Amans, B. Mahler, M.-F. Joubert, Ch. Dujardin, G. Ledoux and Sh. Mishra, *ACS Appl. Nano Mater.*, 2023, **6**, 2310.
16 T. Boyle, D. Yonemoto, J. Sears, L. Treadwell, N. Bell, R. E. Cramer, M. Neville, G. Stillman and S. Bingham, *Polyhedron*, 2017, **131**, 59.
17 D. Grebenyuk, N. Ryzhkov and D. Tsymbarenko*, J. Fluor. Chem.*, 2017, **202**, 82.
18 R. D. Shannon, *Acta Cryst*., 1976, **A32**, 751.